Review Article

Andrea Mele*

Thirty years of ionic liquids: a personal perspective

https://doi.org/10.1515/pac-2025-0440
Received February 16, 2025; accepted June 17, 2025

Abstract: Over the past 30 years, ionic liquids (ILs) have emerged as a versatile class of compounds, bridging fundamental research and applied chemistry. This work offers a historical perspective on ILs, mainly covering fundamental and structural aspects, filtered through the author's personal experience and with no claim of completeness, focusing on four milestone topics: nanostructuring at the mesoscopic level, nanostructuring at the atomic level via intermolecular nuclear Overhauser effect (NOE) studies, the unexpected ability of ILs to selectively dissolve gases, and their potential in promoting sustainable chemistry. These aspects have expanded our understanding of ILs beyond their initial classification as merely molten salts. Among the many challenges ILs face, sustainability is a key factor shaping their present and future applications. As environmental policies evolve, IL-based processes must be evaluated through life cycle assessment and green metrics. However, sustainability extends beyond toxicity and biodegradability, requiring a broader assessment of ecosystem impact and societal acceptance. Addressing these challenges demands a multidisciplinary approach, integrating chemistry with environmental science and engineering. By embracing these perspectives, ILs can continue to drive greener and more efficient chemical processes in the 21st century.

Keywords: biomass treatment; gas solubility; ionic liquids; ISSP21; nanostructuration; NMR spectroscopy; sustainability.

Introduction

There are two common themes in the scientific literature on ionic liquids (ILs) that appear frequently in research articles, reviews, communications, and conference presentations. The first is the "exponential growth" in the number of publications that mention "ionic liquids," often shown as a histogram. The second is a bullet-point list highlighting the positive properties of ILs, such as low vapor pressure, non-flammability, high chemical stability, a large liquidous range, and a wide electrochemical window. These recurring themes in ILs literature serve as markers of the significance and popularity of this class of compounds. The scientific literature already offers detailed and comprehensive reviews on the fundamental aspects of ILs and their applications,[1–12] and this review does not intend to duplicate that work. Instead, the aim here is to reflect on the evolution – over the last thirty years – of certain concepts and achievements that, in the author's subjective view, represent important, fascinating, and distinctive aspects underlying the success of ILs. Following a brief historical introduction leading to the so-called second generation of ILs, this work will focus on four key milestones in the study of ILs. First, the *nanostructuring* of ILs, which refers to the mesoscopic consequences of their molecular characteristics that make them much more than just molten salts. Second, the *quantitative evaluation of intermolecular interactions* that lead to nanostructuring. In this part, the significant development of the theory behind the nuclear Overhauser

Article note: A collection of invited papers based on presentations at the 21st International Symposium on Solubility Phenomena and Related Equilibrium Processes (ISSP21) held on 9–13 September 2024 in Novi Sad, Serbia.

***Corresponding author: Andrea Mele**, Department of Chemistry, Materials and Chemical Engineering "G. Natta", Politecnico di Milano, Piazza L. da Vinci 32 – 20133 Milano, Italy, e-mail: andrea.mele@polimi.it. https://orcid.org/0000-0002-0351-0538

effect (NOE) applied to ILs will be critically examined, with the help of case studies. Third, the *ability of ILs to dissolve gases*, often in a selective manner. This property will be discussed in relation to local ordering, creating a connection with the previous section. Finally, the *contribution of ILs to the advancement of 21st century chemistry*, particularly in promoting renewable sources of carbon atoms, will be briefly highlighted.

Prehistory and history of ILS

If we consider the widely accepted definition of an ionic liquid (IL) as an ionic compound with a melting point below the boiling point of water at atmospheric pressure, the earliest examples of ILs can be traced back to 1888 and 1914. [13] Some remarkable examples are sketched in Scheme 1. In their pioneering work, Gabriel and Wiener [14] noted the unusually low melting point (52 °C) of ethanolamine nitrate, placing it within the general properties of propylamine derivatives. Around the same time, Paul Walden included ethylammonium nitrate (EAN), a salt with a surprising melting point of just 12 °C, in his broader investigation titled "On the molecular size and electrical conductivity of some molten salts".[15] Chemistry at the turn of the 19th and 20th centuries was not yet advanced enough to anticipate the profound impact of these low-melting salts on the fundamental understanding of matter assembly and organization, nor their potential technological applications as early ILs. Indeed, it took 94 years after Walden's publication to demonstrate that the network of intermolecular interactions in EAN resulted in the first instance of nanostructuring in an IL with an alkyl chain shorter than four carbon atoms.[16] The modern term "ionic liquids" and the emergence of the so-called first generation of ILs[1] can be traced to 1978, when Osteryoung introduced butylpyridinium chloroaluminate.[17] A few years later, alkylimidazolium chloroaluminates were also introduced.[18] Early research on ILs was primarily focused on applications, largely overlooking the significant drawbacks of using strong Lewis acids like $AlCl_3$ and the high temperatures required for the practical use of chloroaluminate ILs in energy storage devices. The issue of ILs instability to air and humidity was successfully addressed in 1992 by Wilkes and Zaworotko. They used simple metathesis reactions on ethylmethylimidazolium iodide [EtMeim]I to prepare air and water stable ILs such as [EtMeim]NO_3, [EtMeim]BF_4, [EtMeim]$MeCO_2$, [EtMeim]$_2SO_4{\cdot}H_2O$.[19] The authors not only paved the way to the second generation ILs (see Scheme 2 for a selection of the most common ILs), but also set the foundation for the rational understanding of the mechanisms underlying both liquidous range and nanostructuration: "*It is clear from this study that EtMeim$^+$ is an ideal candidate for general use in ionic liquids. It is of moderate size (thereby lowering lattice energies), its shape appears to promote cation stacking, it is facile and inexpensive to prepare, chemically and electrochemically robust, and can only engage in the thermodynamically weak C–H···X hydrogen bonding*".[19] This conclusion anticipated the rigorous answer to the question "Why are ionic liquids liquid?" proposed in 2008 by Krossing et al.[20] The authors assessed the $\Delta_{fus}G°$ of a collection of ILs through a Born-Fajans-Haber cycle (Fig. 1), and draw the clear-cut conclusion that "*The negative $\Delta_{fus}G°$ values obtained for all ILs indicate that these salts are liquid at ambient temperatures […] due to the large size and conformational flexibility of the ions, which leads to small lattice enthalpies and large entropy changes that favor the liquid state.*"[20] The iconic pictures reported as Fig. 2[21] summarizes the complex and appealing connection between molecular features and macroscopic behavior: The melting point trend of 1-methyl-3-alkylimidazolium PF_6 indicates the competition between the symmetry breaking effect of the alkyl chain – opposing to the coulombic attraction and destabilizing the crystal packing – and the attractive dispersive interactions, whose effect predominates over the "packing frustration" starting from C6. Overall, this is the *preludio* to the main theme of the local structuration of ILs.

The magic of ILs: nanostructuration

The ILs have distinctive aggregation motives fingerprinting their physical chemistry. An exhaustive survey can be found in refs. 9, 10, which also highlight the large variety of spectroscopic and theoretical methods used to investigate the microheterogeneity in ILs. In this section I will focus on some paradigmatic achievements reported by neutron scattering, X-ray scattering and molecular dynamics. Considering the second generation ILs,

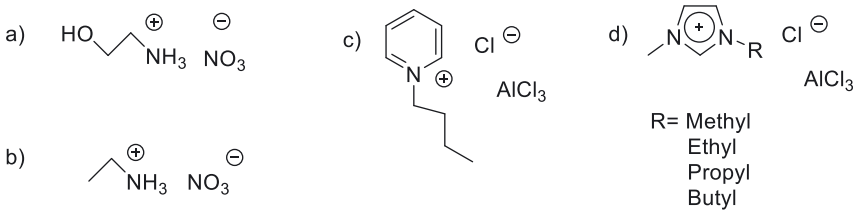

Scheme 1: Structures of compounds mentioned in the Prehistory section: (a) ethanolammonium nitrate, ref. 14; (b) ethylammonium nitrate (EAN), ref. 15; (c) butylpyridinium chloroaluminate, ref. 17; (d) alkylimidazolium chloroalumiminates, ref. 18.

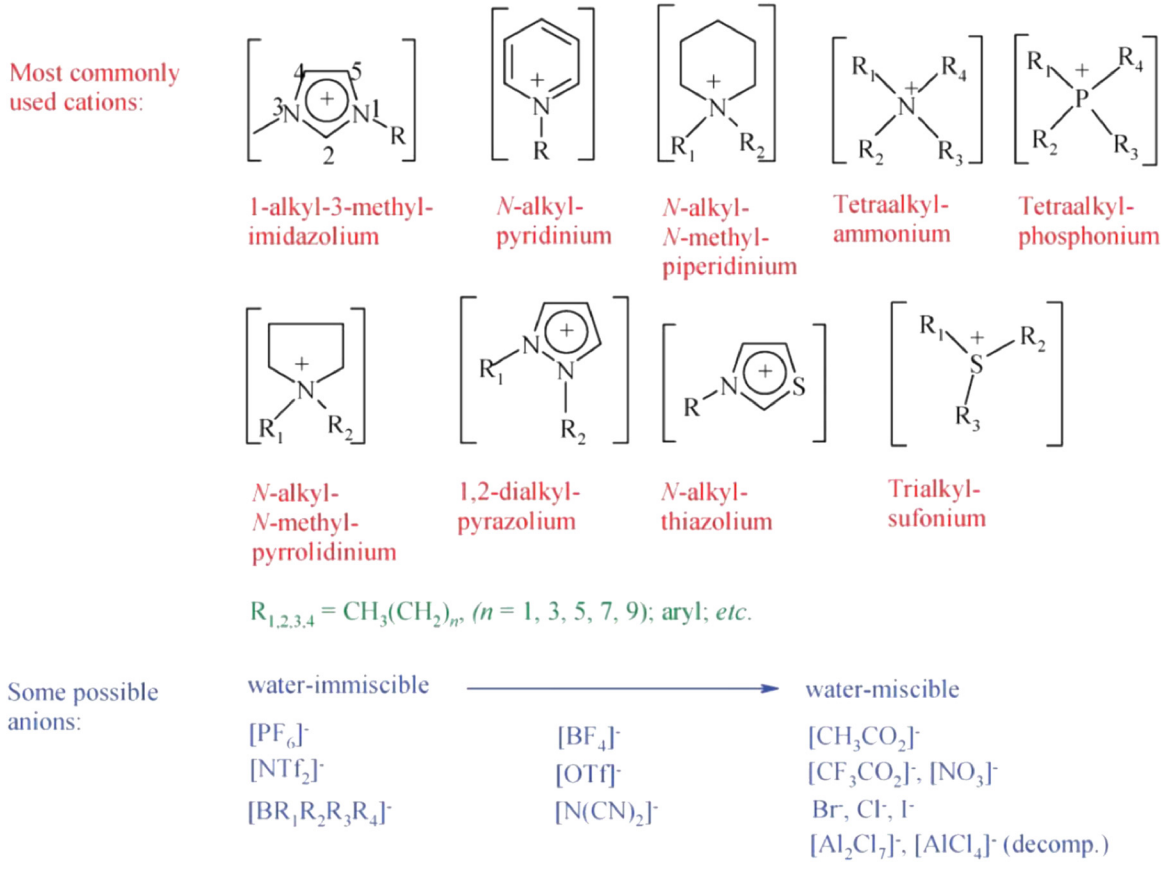

Scheme 2: Sketch of the structure of the most common second generation ILs. Reprinted with permission from ref. 12 Copyright © 2008 Royal Society of Chemistry.

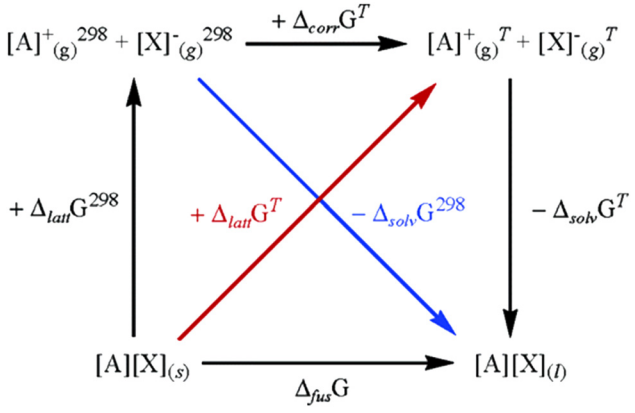

Fig. 1: The Born-Fajans-Haber thermodynamic cycle to calculate $\Delta_{fus}G°$ of selected ILs. Adapted with permission from ref. 20. Copyright © 2006 American Chemical Society.

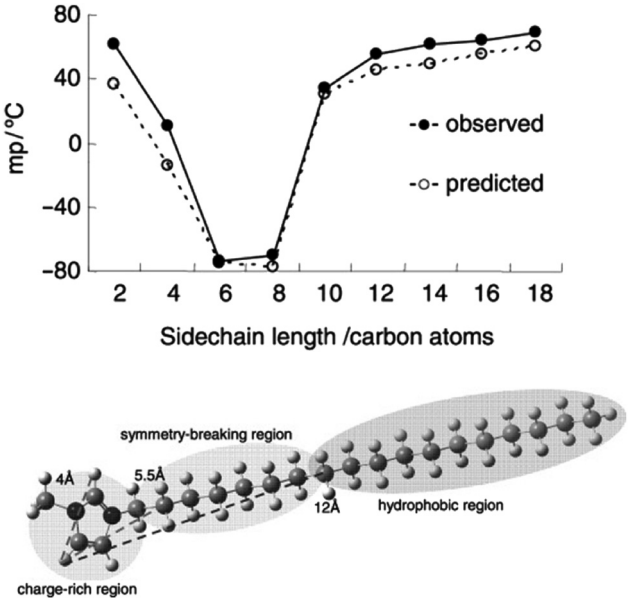

Fig. 2: Top: mp of methylalkylimidazolium PF_6 as a function of the number of C atoms in the alkyl chain. Bottom: optimized geometry of 1-methyl-3-octadecylimidazolium cation with the regions affecting the melting point trend. From ref. 21. Copyright © 2007 WILEY-VCH Verlag GmbH & Co. KGaA, Weinheim.

the milestone work on neutron scattering of symmetric dimethylimidazolium ($dmim^+$) salts from the group of Hardacre highlighted similarity and differences between the crystallographic order detected in the solid state and the local order in the liquids state, largely modulated by size, shape and electron distribution of the anion, have been highlighted.[22] The discovery that the anions' structure influenced the first and second solvation shells sets the bases of the tunability of ILs properties according to the structure of the components. Figure 3 summarizes some key points in the paradigmatic example of chloride, PF_6 and bis-trifluoromethylsulphonyl imide (TFSI) anions. The surfaces show the probability of finding an ion with respect to the central imidazolium cation, considering both the cation – anion and the cation – cation shells. The mutual disposition of chloride – dmim and PF_6 – dmim are opposite, showing the dominant point-charge behavior of Cl^- leading to the strong C(2)–H···Cl hydrogen bond on the one side, and the purely coulombic interaction of dmim and PF_6 on the other. The distribution obtained for the dmim TFSI is driven by the high degree of charge delocalization and increased size of the anion. The probability surfaces show an increasing contribution of anion – cation mutual exclusion in the order $Cl < PF_6 << TFSI$. A good similarity between the liquid structuration and some crystallographic features was reported in the case dmim Cl whereas, on the opposite, no correlation was observed and reported in the case of dmim TFSI. The role of the alkyl chain in imidazolium-based ionic liquids was the object of a milestone paper[23] that introduced, in 2006, the nowadays consolidated concept of polar – apolar domains as source of micro-heterogeneity in isotropic ionic liquids. The investigation, carried out by molecular dynamics simulations,

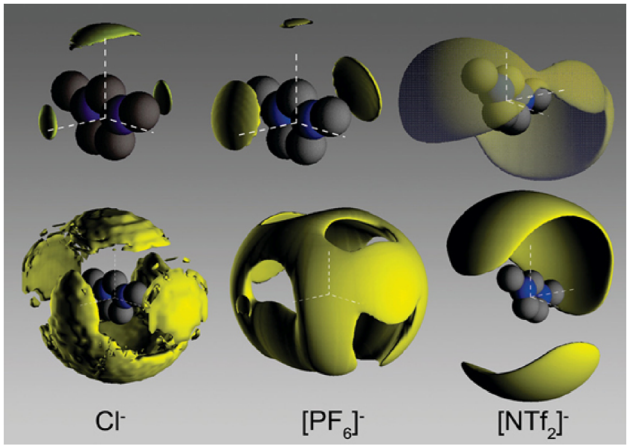

Fig. 3: Top: probability surface for anion around central imidazolium cation. Surface encloses top 5 % anions. Bottom: probability surface of imidazolium cations around central imidazolium ion. The surfaces enclose the top 20 % of molecules each in the distance range 0–9 Å. Reprinted with permission from ref. 22. Copyright © 2007 American Chemical Society.

demonstrated the tendency of the polar parts of the IL – the imidazolium ring and the counterion – to aggregate via coulombic interactions, and the apolar tails to segregate into domains whose size and interconnection increased with the number of C atoms of the alkyl chains and driven by dispersive interactions. The visual description of the progressive formation of the polar – apolar domains is reported in Fig. 4, actually one of the most iconic pictures in the history of ILs, due to the communication efficacy associated to the color code selected by the authors to designate the opposite domains (red: polar, green: apolar), and coincident with the colors of their own country flag. Figure 4 shows how the polar components arrange in a three-dimensional network of ionic channels, while the apolar domains progressively evolve from a dispersed microphase with C2 alkyl chains to a continuous, interconnected phase for longer chains (C6 → C12), with C4 setting the border for the two regimes.

Experimental evidence for nanoscale segregation in ILs were proposed in 2007 by using X-ray scattering.[24] Figure 5 shows the experimental scattering profile obtained on 4 different methyalkylimidazolium chlorides with increasing alkyl chain length (Cn with n = 3, 4, 6, 8, 10). The featureless curve displayed in the case of C2 progressively transforms into a profile showing a clear interference peak, pointing toward the existence of a correlation length L introduced by the alkyl chain. The position of the maximum shifts toward smaller Q – i.e. longer correlation lengths – with increasing n, while, at the same time, the peak gets sharper and more intense. The L values extracted via the Bragg's equation do provide an excellent linear correlation with the n values, consistent with nanometric ordering introduced by the growing alkyl chains. The generality if the L versus n correlation was tested with BF_4^- analogues (Fig. 5, right panel). Also, in that case the experiments confirmed n = 4 as the critical length for nanoscale segregation. The correlation distances calculated fitted the linear correlation of Fig. 5, left panel, confirming the role of the alkyl chain decoupled from the anion type.

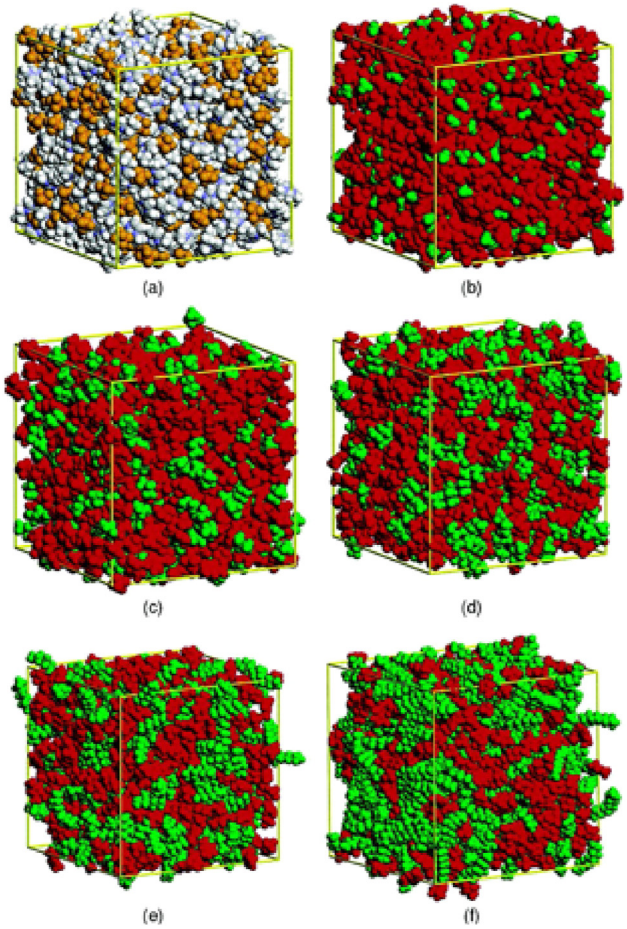

Fig. 4: Simulation boxes for [$C_n$mim][PF_6]. Panel (a) shows a snapshot of the MD of [C_2mim][PF_6] with CPK graphics and conventional colors. Panels (b) to (f) show a snapshot of MD simulations of [$C_n$mim][PF_6] with n = 2, 4, 6, 8, 12, in the order. The color code is green for apolar domanins and red for charged domains. The use of red/green colors guides the eye to the detection of the progressive increase of domain size with increasing n. Reprinted with permission from ref. 23. Copyright © 2006 American Chemical Society.

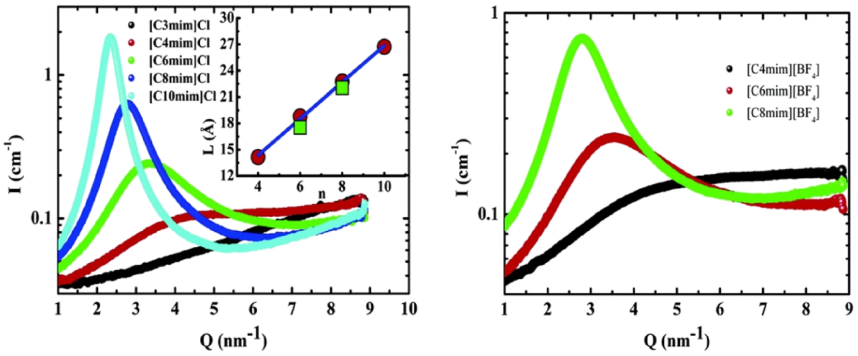

Fig. 5: Left: X-ray diffraction profiles for a series of methylalkylimidazolium chlorides: [C*n*mim]Cl, with n = 3,4,6,8,10 at 25 °C. The inset reports the linear correlation between the alkyl chain length and the measured spatial correlation $L = 2\pi/Q_{max}$ in Å. Q_{max} is the momentum transfer corresponding to the interference peak. The circles indicate the correlation points found for the [C*n*mim]Cl while the squares refer to selected [C*n*mim][BF_4] (squares). Right: X-ray scattering intensity plots for selected [C*n*mim][BF_4] at 25 °C. Reprinted with permission from ref. 24. Copyright © 2007 American Chemical Society.

In a sufficiently large Q range, ILs usually show three distinct features in the X-ray small/wide angle (SWAXS) profile: a prepeak in the range 0.2–0.6 Å^{-1}, a second peak between 0.5 and 1.0 Å^{-1}, and a third feature between 1.0 and 2.5 Å^{-1}. A crystal-clear physical interpretation of these interference peaks can be found in refs. 25, 26, while Fig. 6 shows the concept in a pictorial way. The key importance of the prepeak for the assessment of the local structuration of ILs was stressed by the authors. Indeed, the existence of a prepeak "*is indicative of polar–apolar alternation* […] *linked to structural heterogeneity*", thus "*a missing prepeak is often indicative of small apolar components and a lack of polar–apolar alternation. A missing intermediate peak is likely due to cancellations because at room temperature charge alternation is always present.*"[26] From a different viewpoint, an appearing prepeak is diagnostic of a structural transition. Figure 7 provides an example of this.[27] The overlayed profiles follow a variable T observation carried out on a pyrrolidinium based IL with the perfluorinated anion IM_{24} (TFSI analogue with perfluorinatd ethyl and *n*-butyl side chains). The reversible appearance of a feature at T = –55 °C and centered at Q = 0.48 Å^{-1} points toward the formation of fluorous domains due to segregation of fluorinated

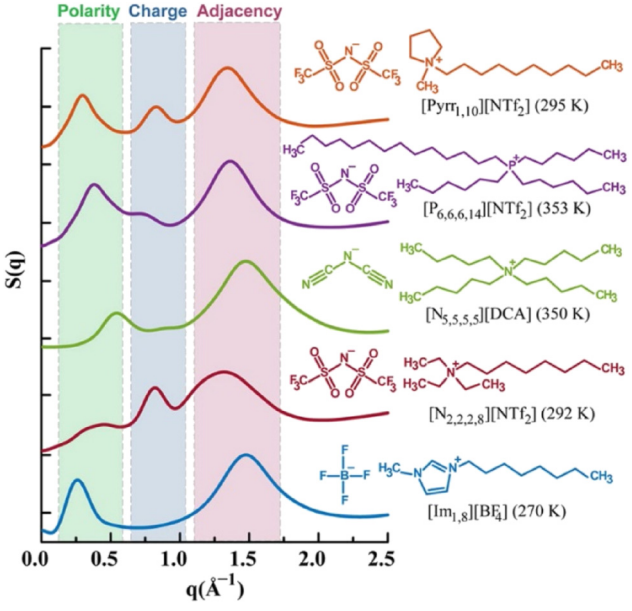

Fig. 6: Simulated SWAXS profiles of paradigmatic ILs highlighting the three common features. The peak observed at higher q values corresponds to adjacency correlations between nearby atoms, which arise from both intermolecular and intramolecular interactions. The intermediate peak reflects charge alternation, while the smallest q value peak results from polarity alternation, indicating structural heterogeneity. The lack of a charge alternation peak, as seen in [$Im_{1,8}$][BF_4], does not imply the absence of this symmetry; rather, it signifies complete cancellation of peaks and antipeaks at this specific q value. For a discussion of the origin of peaks and anti-peaks see ref. 25. Adapted with permission from ref. 26. Copyright © 2015 American Chemical Society.

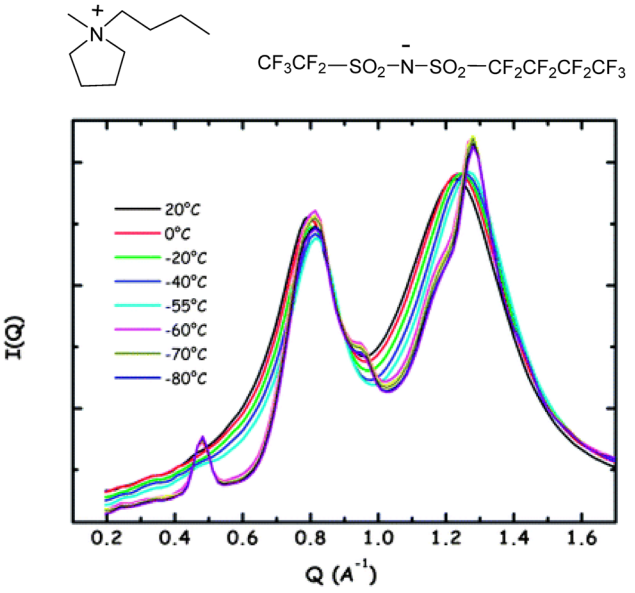

Fig. 7: Small and wide angle X-ray scattering (SWAXS) intensity profiles of 1-butyl,3-methylpyrrolidinium [IM24] in −80 °C < *T* < 20 °C temperature range. The peak at $q = 0.48$ Å^{-1} is detectable for *T* < −55 °C and it is consistent with the formation of fluorous tails clusters. Adapted with permission form ref. 27 Copyright © 2013 Royal Society of Chemistry.

tails once the translational dynamics has been dumped at low T. This research broads the repertoire of nanodomains within ILs, setting fluorophilic domains in the toolcase with polar and apolar domains. The applicative consequences of the possibility of fluorous domains in ILs will be clarified in the next sections.

The NOE saga: measuring the contacts

In 1952, a rather sectorial and visionary paper titled "Polarization of nuclei in metals"[28] paved the way to an unthinkable set of applications in nuclear magnetic resonance spectroscopy, from protein structure to the most recent dynamic nuclear polarization (DNP), and spotlighted on a scientist whose name is now ubiquitous in the never-ending catalogue of NMR acronyms: Overhauser.[29] Indeed, the tremendous technology advancement of NMR instrumentation and software, along with the capillary educational efforts for the dissemination of NMR culture in the chemical community, made easily available sophisticated experiments such as NOESY, ROESY, HOESY (all of them embedding the "O" of Overhauser) and variants even to undergraduate students as irreplaceable physical method for the assessment of three-dimensional structure of molecules in synthetic chemistry[30,31] and biochemistry.[32]

A "nuts and bolts" illustration of what the chemical applications of the Nuclear Overhauser Enhancement (NOE) relies on the basic concept of mutual relaxation ("cross relaxation", here henceforth indicated with σ and expressed in s^{-1}) occurring among nuclei close in space and thus connected with configurational, conformational and assembly features of the molecular architecture. The observation of NOE – as, for instance, correlation peaks in a 2D NOESY experiment or in its rotating frame variant, ROESY – is due to dipolar interactions. These, in turn, decay rapidly with increasing distance *r* of the interacting nuclei (r^{-6} distance dependency), and are sensitive to the dynamic regime, generally expressed by the product $\omega\,\tau_c$ of the nuclei Larmor frequency ω and the rotational correlation time τ_c, in first approximation the time needed for a molecular rotation of one radian under random thermal tumbling. The distance dependence of NOE intensity, in particular, is the conceptual gate to the measurement of internuclear distances in solution. The limiting factor is assumed to be the distance threshold of 5 Å for vanishing NOE. This property paves the way to measure internuclear distances in the liquid, i.e., to use the NOE as a "proximity ruler".

Whitin these premises, the first attempt of assessing the nanostructuration of ILs using the NOE proximity ruler came from the group of Osteryoung in 1995.[33] The authors studied the ROESY pattern in 1-ethyl-3-methylimidazolium $(Emim)^+$ chloroaluminate in the melt state. For the sake of clarity, and for the

non-NMR-specialist reader, also the rotating frame NOE will be referred to as NOE (and not as ROE, with no comment in this article on the similarities and differences between NOE and ROE). In order to distinguish *intra*molecular short contacts – i.e. *intra*molecular NOEs, linked to the imidazolium geometry – and the *inter*molecular contacts – i.e. *inter*molecular NOEs, originated by cation-cation assembly due to nano-structuration – the authors synthesized the homologue IL based on the fully deuterated cation (Emim-d_{11})$^+$ and mixed the pristine and the deuterated ILs in molar ratio 5:95. In this way, each (Emim)$^+$ was totally surrounded by (Emim-d_{11}) species, resulting in the complete quench of the intermolecular NOEs. Figure 8 shows the two-dimensional contour plot of the ROESY experiment carried out on the pristine IL and the 95:5 deuterated mixture. The comparison of the correlation peaks (cross-peaks originated by NOE between H nuclei in space proximity) detectable in the pure IL and in the mixture of protium and deuterated IL allowed the authors to distinguish intermolecular and intramolecular NOE. On this basis, the authors gave the first evidence of local structuration of an IL in the liquid state without solvent added, presumably due to the H-bond network connecting the imidazolium cations and the chloride anions.[33] In the subsequent years, a different ROESY-based strategy to investigate the network of interactions driving imidazolium-based ILs' local ordering was proposed. The emblematic IL 1-butyl-3-methylimidazolium BF_4 [Bmim][BF_4] was added of known amount of water used as competing agent to the intermolecular interactions.[34,35] The structural changes on the bulk IL were monitored by volume integration of the ROESY cross-peaks. The observed trends are reported in Fig. 9. The histogram displays two different regimes: the H pairs corresponding to intermolecular contacts (as worked out in ref. 33) showed negative bars, indicating weaker NOE intensity with increasing water content, whereas the positive bars highlighted the opposite behaviour affecting the H pairs characterized by intramolecular NOE. The two opposite response to the growing water concentration point towards water molecules interacting with the polar domain, making the imidazolium-imidazolium association looser, possibly by competing for the C–H···F hydrogen bond.

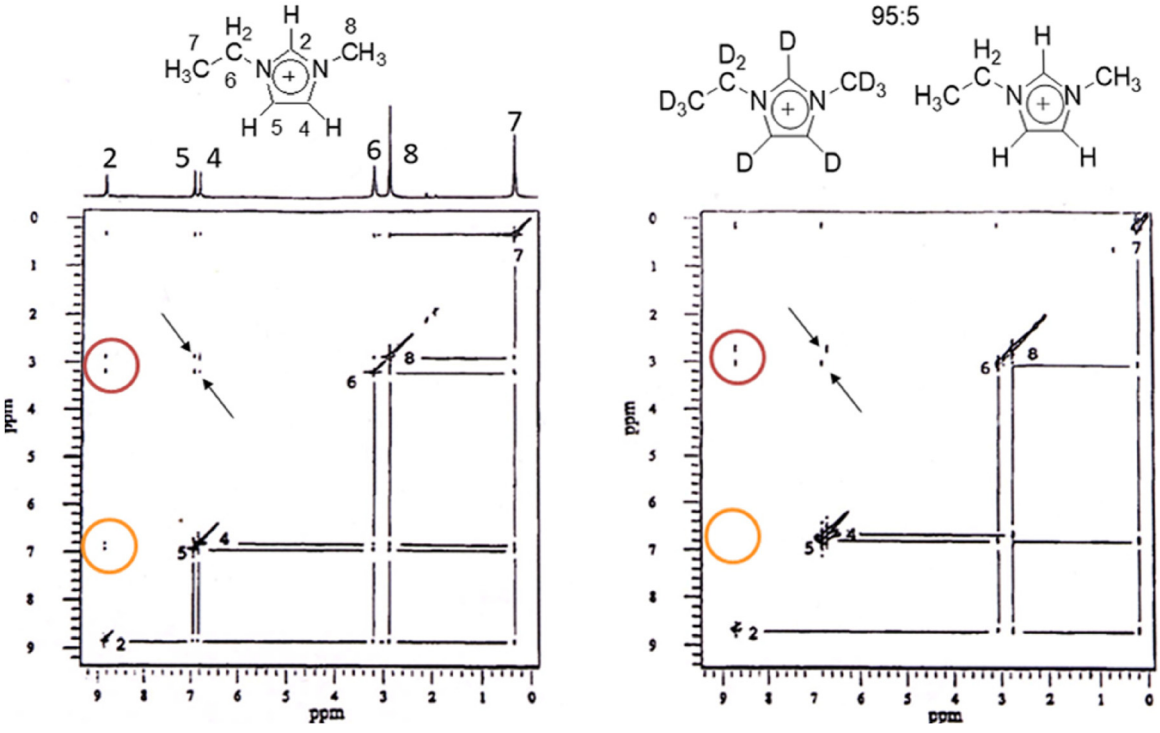

Fig. 8: Left panel: molecular formula, atom number of the Emim$^+$ cation with the contour plot of ROESY experiment. Peak assignment is reported for the one-dimensional projection and on the diagonal. On top of the right panel are reported the molecular formulae of protium and deuterated Emim$^+$ cations, used by the authors in 95:5 M ratio. The orange circle and the arrows indicate the cross peaks that disappeared after dilution of the protium IL with the deuterated analogue, consistent with the intermolecular short contacts. Adapted with permission from ref. 33 Copyright © 1995 American Chemical Society.

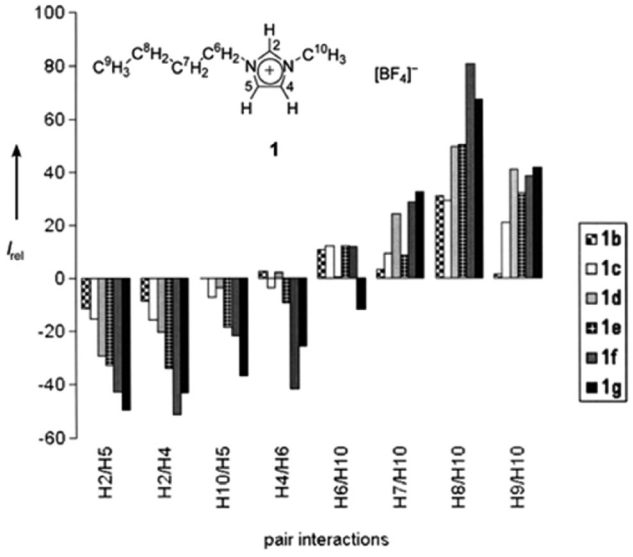

Fig. 9: Relative intensities of intermolecular ROESY cross-peaks in samples **1b**–**g**. The samples were prepared from pure **1a** (x_{water} **1a** = 0) by adding a suitable amount of water to obtain the following water molar fractions x_i: 0.09, 0.17, 0.27, 0.36, 0.45, 0.52 for **1b** to **1g**, in the order. The relative intensity (%) is defined as $I_{rel} = [(V - V_0)/V_0] \times 100$, with V_0 is the integrated volume of a specific cross-peak in sample **1a**, and V is the integrated volume of the same cross-peak **1b**–**1g**. All volumes are internally normalized against the H2–H10 cross-peak, which is assigned a value of 1.00 (arbitrary units). A negative bar for a given cross-peak indicates a reduction in relative intensity compared to the corresponding cross-peak in the pure ionic liquid. Reprinted from ref. 34 with permission and under the terms of the Creative Commons Attribution (CC BY).

In turn, the augmented polarity experienced by the butyl chain with growing water concentration seems to reinforce the chain-chain interaction within the apolar domain, leading to increased NOE intensity.[34,35]

An attempt of measuring intermolecular dintances inside the polar domain of representative 1-butyl-3-methylimidazolium BF_4 [Bmim][BF_4] and 1-butyl-2,3-dimethylimidazolium BF_4 [Bdmim][BF_4] was reported in 2006.[36] The methodological approach was based on the measurement of the NOE kinetics by using an array of NOESY experiments with incrementing mixing time τ (i.e. the time interval within NOESY the pulse sequence in which the dipolar interaction leading to NOE is allowed to occur) and extracting the cross-relaxation rate σ from the slope of the NOE build-up curve for $\tau = 0$. The data showed unexpected resemblance of some of the intermolecular distances measured in the pure liquid with the corresponding ones in the solid state via single-crystal X-ray diffraction. This finding confirmed the existence of local structure in the pure ILs and alligned with early discoveries from X-ray scattering [see previous section]. In 2012 a sistematic investigation from the group of Giernoth and based on heteronuclear ^1H–^{19}F NOE data highlighted an impressive matching of the NOE-derived intermolecular contacts with those predicted via molecular dynamics.[37] These works assumed more or less tacitely that the formation of suitable aggregates of the IL's components – from ion-pairs to more complex supramolecular assemblies – were stable enough to allow the treatment of the intermolecular NOE as intramolecular, i.e. characterized of a single correlation time of the vector connecting the space-close nuclei and rigorously adhering to the r^{-6} distance dependence.[30,31] Although such an assumption fueled – and in part still fuels – the debate on the issue of the actual formation of long-lived aggregates within ionic liquids, at the time of the pubblication of the NOE-extracted intermolecular dinstances, "*that was the state of the art for ILs*".[38] Indeed, the theoretical framework underlying intermolecular NOEs is more intricate than for intramolecular cases. Comprehensive treatments of the theory, which can be conceptually challenging, are detailed in works by Ayant,[39] Furo,[40,41] Gerig,[42,43] Halle,[44] and Bagno.[45,46] Reduced to the bare minimum, the assumptions and main conclusions of the model can be summarized as follows: i) the intermolecular vector $\boldsymbol{r}$ connecting the nuclei undergoing cross-relaxation is modulated by translational diffusion. As a consequence, the randomization time of $\boldsymbol{r}$ is longer compared to the intramolecular case; ii) the predicted distance dependency is r^{-n}, with $1 < n < 6$, depending on the system dynamics; iii) also long-range interactions may give rise to observable intermolecular NOEs. In other words, contacts beyond the first solvation shell may provide observable, long-range NOE. The application of these theoretical framework to model [Bmim][BF_4] was presented in 2013 in a disruptive paper by Gabl, Steinhauser and Weingärtner.[47] On the bases of their simulations, the authors showed how the distance dependency of intermolecular NOE was a function of the Larmor frequency of the interacting nuclei. This conclusion prompted the authors to state that, when measuring and interpreting NOE, "*frequency matters.*"[47] Figure 10 shows one of the graphic outputs of their simulations. To fully understand the disruptive meaning of the

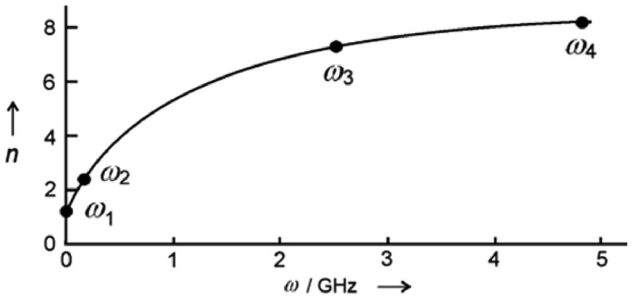

Fig. 10: Graphic representation of the exponent n of the r^{-n} distance dependency of intermolecular NOE intensity as a function of operating frequency. The simulation is obtained for a basic spectrometer frequency of 400 MHz. The reference points ω_1 to ω_4 are set at 1 MHz, 0.15 GHz, 2.5 GHz, and 4.85 GHz, returning n exponents of 1.17, 2.5, 7.2, and 8.2, in the order. The data clearly show the transition from long-range (small exponent) to short range (large exponent) distance dependency of NOE. Reprinted from ref. 47 with permission and under the terms of the Creative Commons Attribution (CC BY).

curve, it is necessary to introduce here the spectral density function $J(\omega)$, a mathematical object containing the cross-relaxation σ_{IS} and describing the modulation of the dipole-dipole interactions of the nuclei developing NOE, here indicated as I and S. The authors pointed out that the overall $J(\omega)$ was a linear combination of $J(\omega_I + \omega_S)$ and $J(\omega_I - \omega_S)$, in turn associated to short-range and long-range interactions, respectively, and that the term $(\omega_I - \omega_S)$ overpowered $(\omega_I + \omega_S)$. In the case of ^{1}H–^{1}H or ^{1}H–^{19}F NOE, the corresponding $(\omega_I - \omega_S)$ are very small, due to the similarity of the Larmor frequencies of I and S, heading to interactions beyond the first solvation shell. On the contrary, heteronuclear NOEs such as ^{1}H–^{7}Li or ^{1}H–^{31}P are expected to truly spot on short contacts, due to the large difference or the Larmor frequency of the nuclides, thus providing the researcher with a unique spectroscopic tool to assess an atomistic picture of solvation.

After 2013, many efforts have been done to refine the acquisition and processing of intermolecular data according to the GSW approach. It is worth noting that the refined fitting of appropriately normalized HOESY build-up curves, using a modified model that incorporates both longitudinal relaxation times and diffusion coefficients, enables accurate determination of absolute intermolecular cross-relaxation rates. This approach, elegant although not straightforward, facilitates comparative analyses across various ionic liquids, concentrations, and temperature conditions.[48–50] The GSW model received some validations, partly based on the comparison of the NOE data and the intermolecular distances available from other methodologies, such as single crystal X-ray crystallography[51] or molecular dynamics.[52,53] The group of Schröder proposed a full simulation of Emim trifluoromethanesulphonate (triflate, TfO) as pure liquid and containing LiTfO.[53] The authors simulated the systems using both fully atomistic and polarizable models, as nonpolarizable force fields tend to exaggerate directed electrostatic interactions in ionic liquids (ILs). In reality, electronic charge distributions adjust during molecular interactions, leading to reduced viscosity in ILs. Consequently, polarizable force fields are essential for capturing realistic pair diffusion dynamics critical to the NOE. Additionally, the NOE were directly extracted from the simulation trajectory, bypassing traditional models and thus avoiding their inherent assumptions. The comparison of experimental and calculated ^{1}H–^{1}H, ^{1}H–^{19}F and ^{1}H–^{7}Li NOEs was exceedingly good and the simulations of the distance dependency of NOE on the Larmor frequency difference of the interacting nuclei fully confirmed the long-range nature of ^{1}H–^{1}H, ^{1}H–^{19}F NOE, and the short-range contribution of ^{1}H–^{7}Li NOEs, as displayed in Fig. 11.

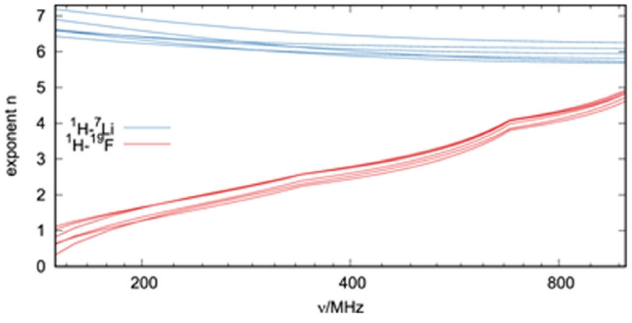

Fig. 11: Plot of the exponent n of the r^{-n} power law for NOE intensity as a function of the magnetic field (in frequency units). The H–Li spins show a distance dependency nearly independent of the magnetic field and consistent with r^{-6} power law. The H–F spin-pairs curves show a marked magnetic field dependency and long-range character at the typical spectrometer frequency. Reprinted from ref. 53 with permission and under the terms of the Creative Commons Attribution (CC BY).

Finally, two critical considerations must be highlighted at the conclusion of this section. First, while the GSW theory has undeniably prompted NMR specialists to reconsider the use and interpretation of NOE in cases of solvation and intermolecular aggregation, the authors may have overlooked its potential to broaden, rather than restrict, the scope of intermolecular NOESY experiments. The long-range nature of certain important classes of intermolecular NOEs, such as $^{1}H–^{1}H$ and $^{1}H–^{19}F$, should not deter chemists from measuring them. Their interpretation contributes to an atomistic understanding that complements the microheterogeneity revealed by WAXS, SAXS, or SANS techniques. As demonstrated previously, the combined application of NOEs, scattering methods, and molecular dynamics (MD) simulations is a powerful investigative tool for studying nanostructured liquids.[52,54] Conversely, the strictly short-range nature of specific heteronuclear NOEs (e.g., $^{1}H–^{7}Li$ NOEs) offers accurate and valuable distance constraints for MD simulations of systems of contemporary interest, such as ionic liquid electrolytes containing dissolved lithium salts.[55]

Second, despite the significant validation of GSW theory through a comparison with experimental data, the debate regarding its general applicability is still open. Notable examples of excellent concordance between NOE-derived structural models and experimental or calculated data exist in the literature without relying on the GSW framework.[56,57] Further research and theoretical advancements are essential to reach a conclusive resolution to this ongoing scientific discussion.

The *Horror Vacui* of gases in ionic liquids

Two primary motivations have driven research into gas solubility in ionic liquids: the need for novel technologies for gas capture, particularly CO_2, and a deeper understanding of how the nanostructuration of ILs influences the mechanisms of gas dissolution. The growing interest in gas capture is largely tied to environmental concerns related to climate change caused by CO_2 emissions. However, research in the early 2000s focused mainly on the engineering aspects of raw gas purification, as CO_2 is the primary contaminant in natural gas streams. Gas-sweetening technologies, based on CO_2 reactions with alkanolamines to form carbonates and carbamates, offer excellent efficiency and (apparently) low costs. Nonetheless, this approach has significant drawbacks, including reagent loss, water transfer to the gas stream, formation of corrosive by-products due to amine degradation, and high energy consumption for regeneration, estimated at 4 GJ per tonne of CO_2.[58,59]

Starting from the first report accounting for the unexpected CO_2 solubility in ILs,[60] ILs have been successfully tested as absorption materials using various strategies. These include the dissolution of gas in bulk ILs for selective CO_2 retention, chemical reactions of CO_2 with task-specific ILs (TSILs), and selective gas separation using supported IL membranes (SILMs).[61–63] This non-exhaustive list also includes the use of polymerized ILs (polyILs) and polyIL-IL composite materials.[64] One particularly intriguing application involves switchable ILs for CO_2 sequestration. In 2005, it was demonstrated that a mixture of the superbase 1,8-diazabicyclo-[5.4.0]-undec-7-ene (DBU) and an alcohol could be reversibly transformed into an IL through the *in situ* formation of a DBUH carbonate with the alcohol. The reaction could be reversed by bubbling N_2 or Ar through the IL, regenerating the starting materials (DBU and alcohol).[65] A smart application of this concept emerged in 2010, where the alcohol functional group was incorporated into the N-alkyl chain of the alkylimidazolium cation. For example, 1-(2-hydroxyethyl)-3-methylimidazolium bis(trifluoromethylsulfonyl)imide ($[Im_{21}OH][Tf_2N]$), Fig. 12) captures CO_2 via its reaction with DBU to form a liquid amidinium alkylcarbonate. The system's recyclability, a key feature for the greenness of ILs, was achieved simply by raising the temperature or bubbling N_2. The key mechanism involves the interaction of a strong proton acceptor (DBU) with a proton donor (the OH functional group on the modified alkylimidazolium cation), forming an IL.[66]

This method was further generalized by the same research group, leveraging the well-known acidity of the C(2)–H site of imidazolium cations.[67] As shown in Fig. 13, the superbase 1,3,4,6,7,8-hexahydro-1-methyl-2H-pyrimido[1,2-a]pyrimidine (MTBD) in its protonated state $MTBDH^+$ has a counterion derived from the functionalization of the imidazolium ring at C(2) with a carbonate functional group. The formation of such a zwitterion involves a nucleophilic attack on the CO_2 carbon by the deprotonated, electron rich C(2) of the imidazolium ring, forming a carbonate functional group. Chemisorption of CO_2 is thereby achieved, in a

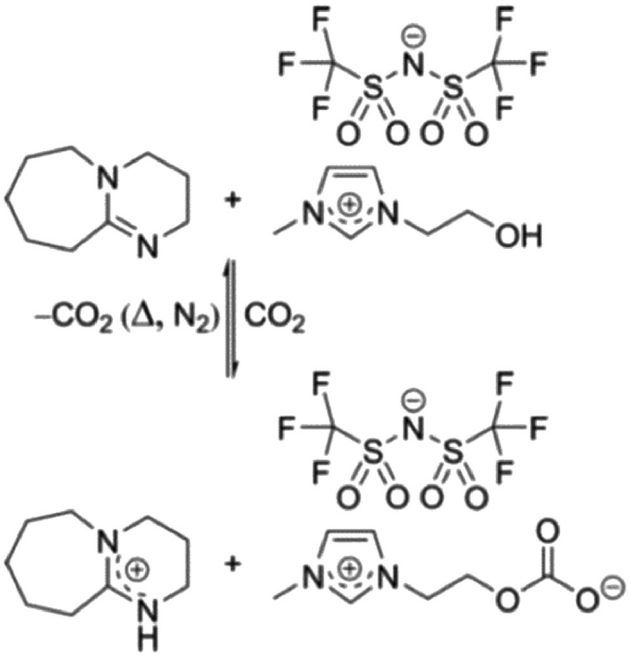

Fig. 12: Scheme of the reaction of superbase 1,8-diazabicyclo-[5.4.0]undec-7-ene (DBU) with hydroxylated imidazolium derivative [$Im_{21}OH$][Tf_2N] in the presence of CO_2. The deprotonated imidazolium forms reversibly the imidazolium carbonate. [$Im_{21}OH$][Tf_2N] and DBU are easily recovered by N_2 bubbling. Reprinted with permission from ref. 66. Copyright © 2010 Royal Society of Chemistry.

reversible way, without prior functionalization of the IL, relying instead on the intrinsic properties of the C atom flanked by N atoms in the imidazolium ring.

Beyond the undeniable practical interest in gas entrapment in ILs, the quest for fundamental knowledge about the mechanism of gas solubility has sparked curiosity among many research teams. With the metaphorical "Hamletic question" – "*Why is CO_2 so soluble in imidazolium-based ionic liquids?*" – A landmark paper[68] explored this topic in depth for the first time. Using molecular dynamics (MD) simulations, the authors explored the local structure of [Bmim][PF_6], [Bmmim][PF_6], and their homologues with the NTf_2 anion, both as pure liquids and in the presence of CO_2. Their findings, pivotal for our understanding, can be summarized as follows (see Fig. 14): i) By defining clever distance descriptors for calculating radial distribution functions g(r), indicative of local order, the study revealed that CO_2 solubility is predominantly driven by CO_2-anion interactions, with the cations playing only a negligible stabilizing role. ii) In an intriguing twist, the presence of 10 mol% dissolved CO_2 in [Bmim][PF_6] or [Bmmim][PF_6] left the anion-cation arrangement unchanged. For instance, the g(r) profile based on the P···C(2) distance between anion and cation remained identical whether CO_2 was present or not.[68] iii) Coupled with calculated densities, this lack of structural perturbation aligns with experimental observations showing no volume expansion of ILs upon CO_2 dissolution. The initial conclusion seemed almost too straightforward: CO_2 occupies the liquid's interstitial voids.

While this "void-filling" argument appears captivating and intuitive, further structural analysis contradicted its simplicity. Huang et al.[69] tackled the void conundrum using Voronoi polyhedral analysis.[70] They demonstrated

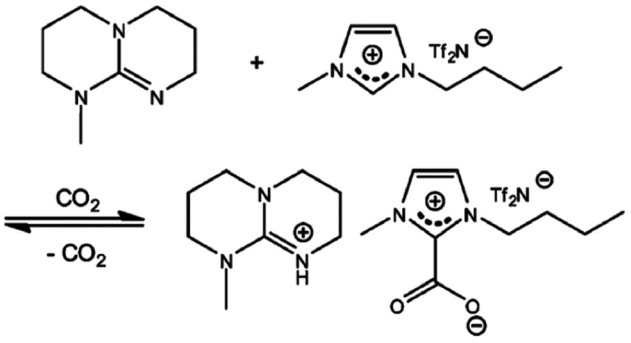

Fig. 13: Deprotonation of C(2) on the imidazolium cation operated by the superbase generates *in situ* the nucleophilic intermediate (not shown in the picture) immediately reacting with CO_2 and generating the final doubly charged ionic liquid. Reprinted with permission from ref. 67. Copyright © 2010 Royal Society of Chemistry.

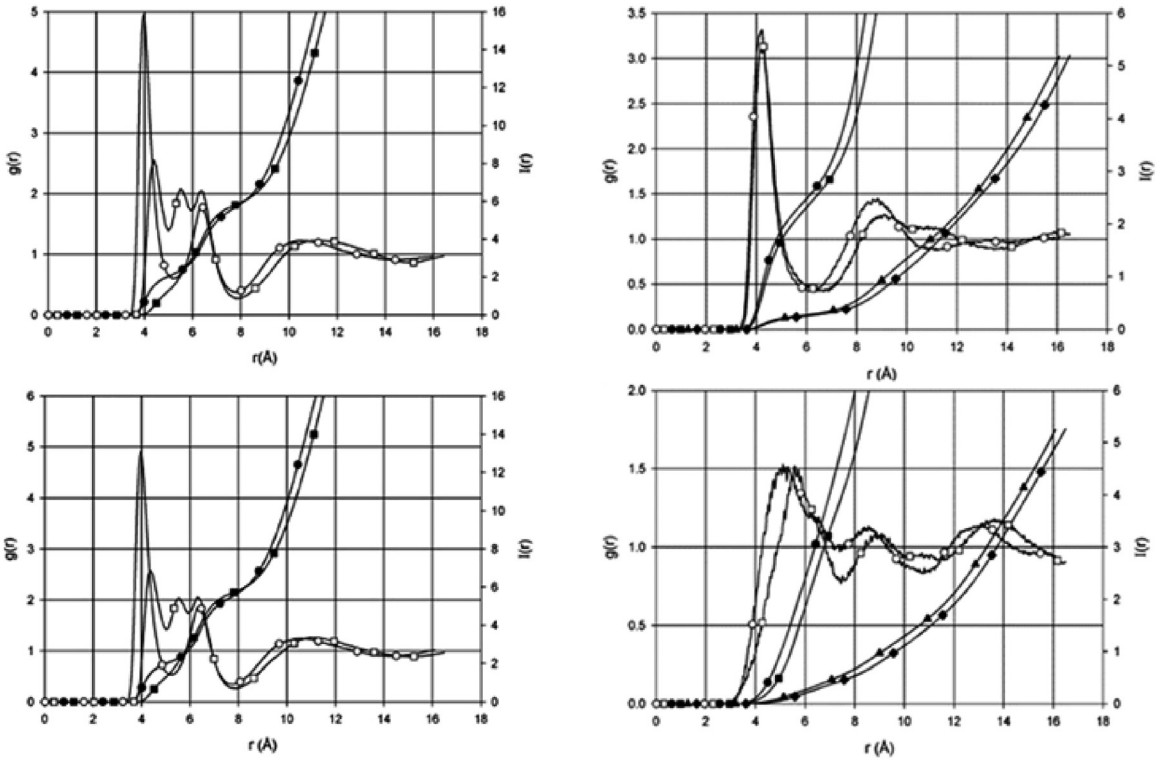

Fig. 14: Top left: The radial distribution functions g(r) and number integrals I(r) illustrate the spatial relationship between the phosphorus atom of the $[PF_6]^-$ anion and the C2 carbon of the cation. The data are represented as follows: g(r) for [bmim] (○), g(r) for [bmmim] (□), I(r) for [bmim] (●), and I(r) for [bmmim] (■). Bottom left: The same analysis is presented for a system containing 10 mol% CO_2. The results indicate that CO_2 does not significantly alter the structural arrangement of cations and anions. Top right: Radial distribution functions and number integrals describing the spatial correlation between the carbon atom of CO_2 and the phosphorus atom in $[PF_6]^-$. The symbols represent: g(r) for [bmim] (○), g(r) for [bmmim] (□), I(r) for the phosphorus atom in [bmim][PF_6] relative to CO_2 carbon (●), I(r) for the phosphorus atom in [bmmim][PF_6] relative to CO_2 carbon (■), I(r) for the CO_2 carbon relative to the phosphorus in [bmim][PF_6] (▲), and I(r) for the CO_2 carbon relative to the phosphorus in [bmmim][PF_6] (◆). Bottom Right: Radial distribution functions and number integrals illustrating the spatial correlations between CO_2 and the N1 nitrogen of the cation. The symbols represent: g(r) for [bmim] (○), g(r) for [bmmim] (□), I(r) for the nitrogen in [bmim] relative to the CO_2 carbon (●), I(r) for the nitrogen in [bmmim] relative to the CO_2 carbon (■), I(r) for the CO_2 carbon relative to the nitrogen in [bmim] (▲), and I(r) for the CO_2 carbon relative to the nitrogen in [bmmim] (◆). Adapted with permission from ref. 68. Copyright © 2004 American Chemical Society.

that the dimensions of existing voids are too small to accommodate CO_2 molecules. Instead, the CO_2 dissolution mechanism in [Bmim][PF_6] involves a subtle angular displacement of the anion relative to the imidazolium ring plane (Fig. 15). This tiny rearrangement does not visibly alter g(r), consistent with,[68] yet successfully creates voids large enough to host CO_2 molecules.

The narrative emerging from these studies paints ILs as liquids teeming with small voids, which rearrange into larger cavities upon the introduction of CO_2. This unique rearrangement enables significant gas dissolution without causing volume expansion. More recently, Shelepova and Medvedev refined this model by conceptualizing interstitial spaces as "empty spheres inscribed between atomic surfaces".[71] Their simulations identified large empty spheres (radius > 0.15 nm) capable of hosting CO_2 molecules. In an unexpected twist, they observed that these large spheres tended to cluster around CO_2 molecules, suggesting that dissolving CO_2 does not merely exploit pre-existing voids – it actively generates additional empty spaces in the IL.

The rigorous definition of "free volume" or "voids" in ionic liquids (ILs) is not as straightforward as it is in polymers, where parameters such as size, shape, size distribution, topology, and connectivity can be explicitly defined.[72] For ILs, Beichel and Krossing[73–75] reported a collection of experimental average local free volume ("hole" volume, denoted as $\langle v_h \rangle$) using positron annihilation lifetime spectroscopy (PALS). This data provides a

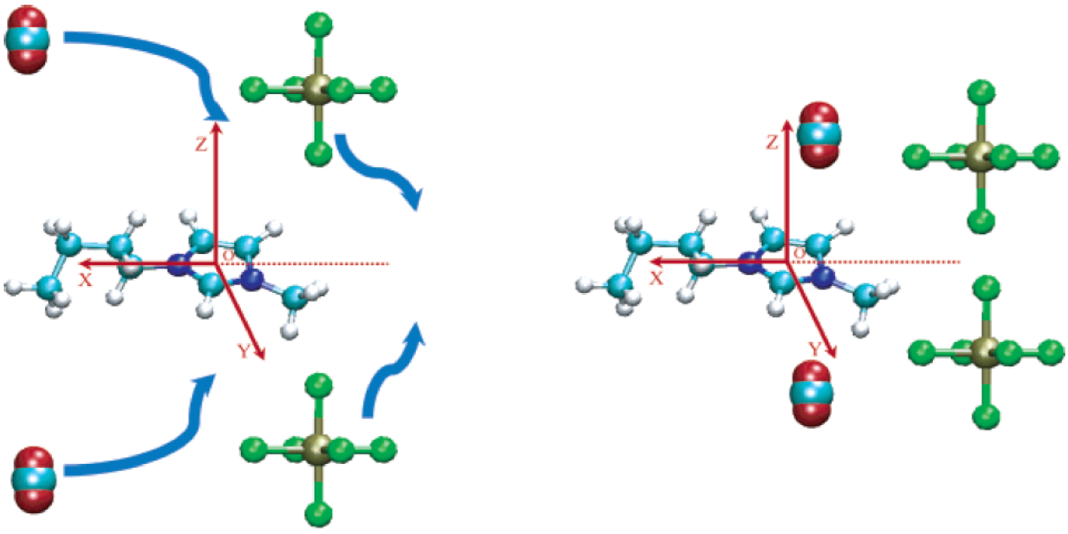

Fig. 15: Proposed model for CO_2 placement [Bmim][PF_6] according to ref. 68. The left panel sketches the initial arrangement of cation, anion and CO_2. The arrows indicate the displacement of CO_2 and anions to reach the final positioning of CO_2, shown in the right panel. Adapted with permission from ref. 69. Copyright © 2005 American Chemical Society.

valuable reference for geometric features, particularly when combined with other physical methods. For instance, ^{129}Xe NMR spectroscopy, known for its sensitivity to compression effects experienced by gas atoms in a porous medium, serves as a molecular probe to explore molecular voids.[76,77]

Measurements on non-ideal IL mixtures, such as $[C_4C_1im][Me_2PO_4]_x[NTf_2]_{1-x}$ and $[C_4C_1im][OTf]_x[NTf_2]_{1-x}$, have shed light on the nature of free volume in ILs, as illustrated in Fig. 16.[78] The average excess hole volume v_h^E (see caption to Fig. 16 for definition) and the excess volume V^E, derived from density measurements, showed a fair correlation, suggesting that the excess mixing volume originates from the average cavity size in the liquid. Similarly, the excess δ^E (see caption to Fig. 16 for the definition) correlated well with both V^E and v_h^E.

This correlation between PALS and NMR data, unprecedented at the time of publication, validated the use of ^{129}Xe NMR as an atomistic probe for free volume in liquids. Despite the vast difference in timescales between the two techniques – seconds for NMR versus nanoseconds for PALS – the results highlight a strong connection between static (PALS) and dynamic (NMR) free volumes. This finding suggests that fluxional processes have a limited influence on the free volume of ILs. Ultimately, the free volume in ILs appears to arise from more persistent structural effects, such as Coulombic and steric interactions, which contribute to the ionic superstructure characteristic of these liquids.[78]

In the final part of this section, the spotlight shifts to a less common but equally important gas: molecular nitrogen N_2. Traditionally, N_2 was regarded as a contaminant in natural gas, similar to CO_2, with its separation presenting a significant challenge due to its well-known chemical inertness and lack of distinct acid-base properties. Recently, however, this perspective has been entirely reversed, as N_2 is now viewed as a virtually limitless and cost-free resource. The renewed interest in N_2 is closely linked to the sustainability challenges associated with NH_3 production, which remains predominantly reliant on the Haber–Bosch process. It is helpful reminding here that the 80 % of worldwide production of ammonia is addressed to fertilizers, the remaining 20 % is used for detergents, drugs, explosives and other products. Additionally, the growing importance of ammonia is also connected to its potential application as energy vector at zero CO_2 emission.

The primary sources of hydrogen for large-scale NH_3 production include hydrocarbons (e.g., methane, biomass, fossil fuels) and water. While using water as a hydrogen source demands significantly more energy than methane (+613.4 kJ/mol N_2), it is more environmentally friendly, avoids greenhouse gas emissions, and conserves finite hydrocarbon resources. These advantages are maximized when the required energy is derived from clean, renewable sources such as solar or wind power.[79]

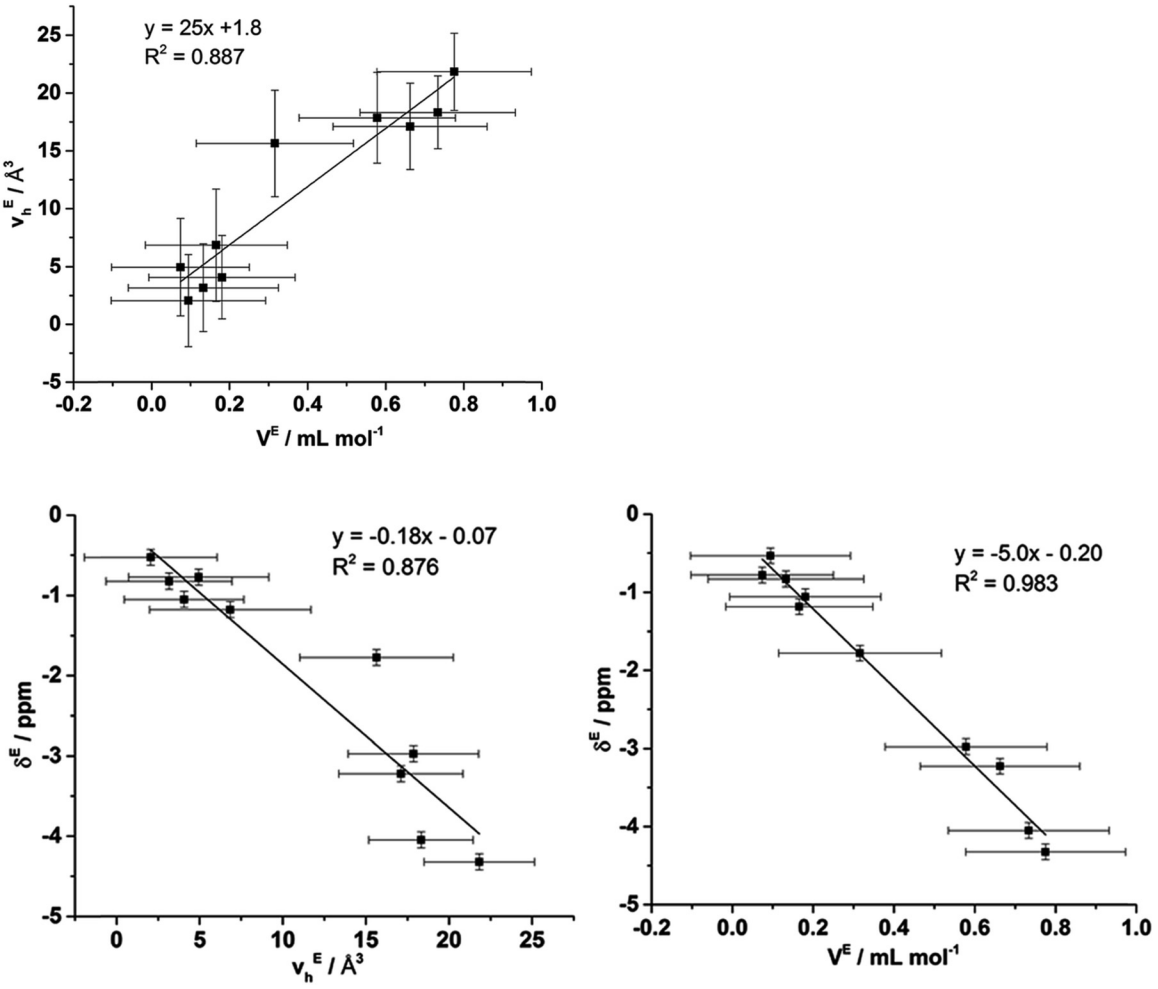

Fig. 16: Top: Plot of the measured excess hole volume v_h^E as a function of the excess molar volume of mixing V^E for the $[C_4C_1im][Me_2PO_4]_x[NTf_2]_{1-x}$ mixtures. The values of v_h^E were obtaind from PALS measurements as difference between the measured hole volume and the ideal value predicted by linear relatinship between the hole volumes determined in the pure liquids. V^E are determined by density measurements. Bottom left: correlation between ^{129}Xe NMR excess chemical shift and v_h^E from PALS measurements from the same mixtures as above. δ^E is defined as $\delta^E = \delta - x_1\delta_1 - x_2\delta_2$, where $x_{1,2}$ is mole fraction of IL 1 and IL 2 respectively, and $\delta_{1,2}$ is the ^{129}Xe chemical shift in pure IL 1 and 2, respectively. Bottom right: correlation between ^{129}Xe NMR excess chemical shift and excess molar volume of mixing V^E for the same mixtures. Reprinted from ref. 78 with permission and under the terms of the Creative Commons Attribution (CC BY).

One of the major challenges in nitrogen reduction reactions (NRR), i.e., the activation of the inert molecular nitrogen to a more reactive N-species, lies in the extremely low solubility of N_2 in aqueous electrolytes (~0.00061 M at 25 °C and 1 atm). This is due to the nonpolar nature of N_2, its strong triple bond, and low polarizability, all of which significantly limit the amount of N_2 available for reaction. Among the strategies developed to enhance N_2 dissolution, the use of non-aqueous electrolytes, such as aprotic ionic liquids, has shown promising results.[80] Specifically, it was highlighted how the presence of fluorous domains in the IL can be a determining factor for good nitrogen solubility. The flourination can be chemically inserted in the alkyl chain of the cation or in the anion or in both. Some authors reported on the role of the cations' structure on the solubility of CO_2 and N_2, both increasing in ionic liquids with fluorinated cations due to the rigidity of the fluorinated chains, which results in a larger free volume.[81] Considering the N_2 solubility as the main target, rather than achieving good CO_2/N_2 selectivity, more recent papers underlined the basic strategy of exploiting the known solubility of N_2 in fluorinated solvents to host N_2 in the fluorinated domains of suitable ILs.[82,83] The rationale behind this is in the structural and electronic properties of N_2 – low polarizability, strong covalent bonds, lack of specific

intermolecular interactions – indicating that a system with scarce tendency to establish van der Waals interactions could fit the principle *similia similibus solvuntur*. Figure 17 offers a graphic summary of these concepts and the results. The authors considered the N_2 solubility in two reference benchmarks (water and $[C_2mim][NTf_2]$) and compared it to those achieved with the ILs shown in the scheme above the histogram. The pale- and dark blue bars indicate the molar solubility of N_2 in two ILs made of a tetraalkylphosphonium cation with fully hydrogenated chains and the anion of perfluorobutylsulphonic acid. The histogram points out that the N_2 solubility is largely exceeding that of the benchmarks and that elongating the perfluoroalkyl chain length from C4 to C8 further improves the solubility. The adjacent two green bars show that the result is practically independent of the type of perfluorinated acid (sulphonic vs carboxylic), thus highlighting the crucial role of the fluorine pool on the anion. This conclusion is confirmed by the last set of bars: the comparison between $[P_{4448}]$ (fully hydrogenated cation) and $[P_{444(8f)}]$ (partially fluorinated cation) shows that the fluorination of the cation is not the determinant

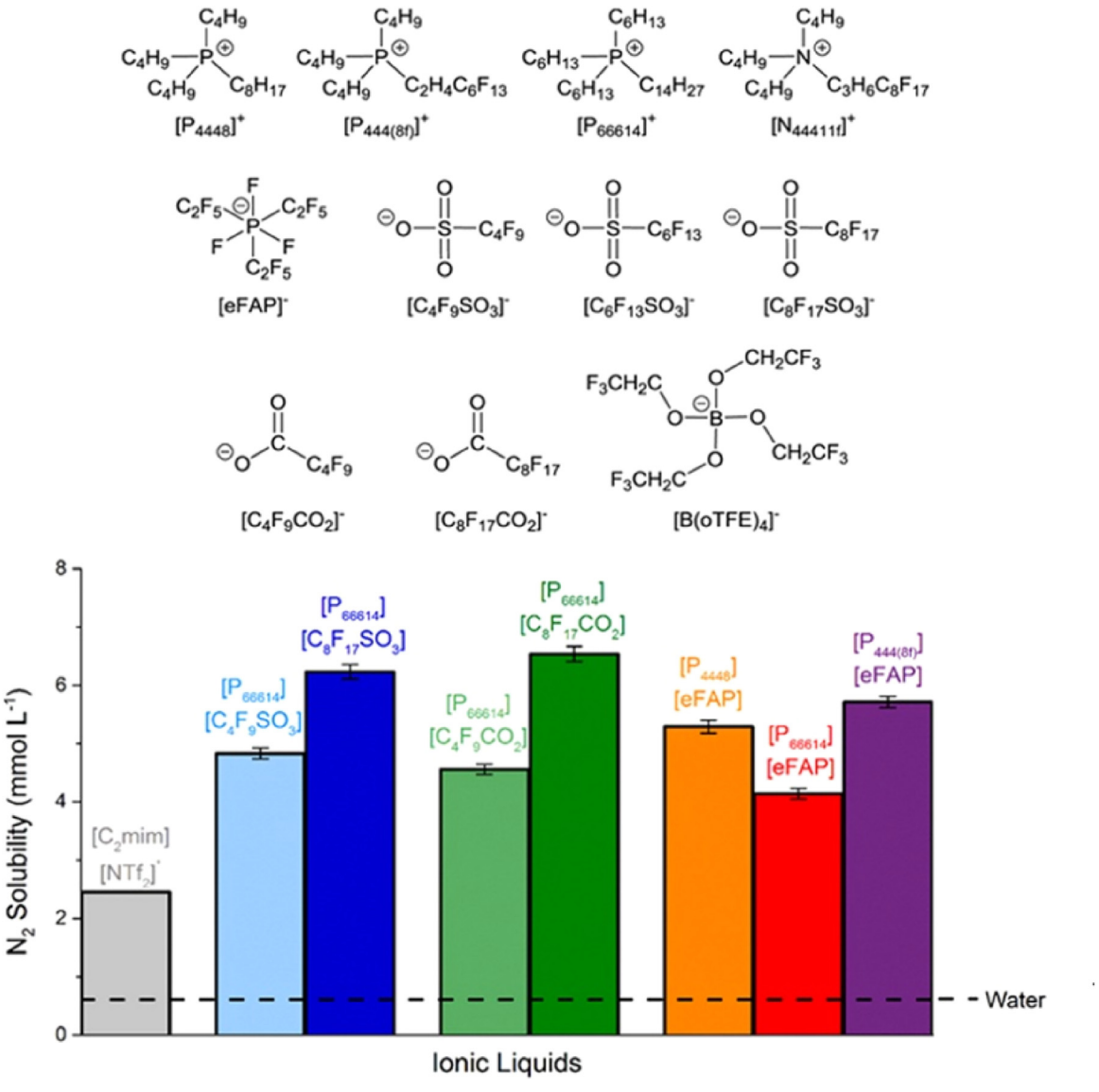

Fig. 17: Top: Molecular formulae of fluorinated ILs for N_2 capture. The histogram shows the N_2 solubility (in mmol L^{-1}) of selected ILs compared to benchmark $[C_2mim][NTf_2]$ (grey bar, left). The dotted line is referred to the N_2 solubility in water. Adapted with permission from ref. 82. Copyright © 2018 American Chemical Society.

factor for N_2 solubility.[82] Overall, the formation of fluorous domains in the ILs paves the way to new classes of non-aqueous electrolytes for up-to-date electrochemical activation of molecular nitrogen.

What are the key factors determining the ability of fluorinated functional groups to influence N_2 solvation and solubility? This question remains open to investigation. A recent study by Li et al.[84] explored this issue using molecular dynamics simulations and free energy perturbation methods to examine N_2 solubility in 20 ionic liquids (ILs), including both traditional and fluorinated types. Using [Emim]NO_3 as the benchmark for N_2 solubility, the study reported a remarkable enhancement – up to 118 times – for the fluorinated IL [Emim]FAP.

The authors identified two key, interconnected factors driving this solubility boost: (i) the presence of at least 10 C–F bonds per IL formula, and (ii) exothermic solvation. In contrast, ILs with fewer C–F bonds and endothermic solvation exhibited significantly lower N_2 solubility. These observations were encapsulated in a newly proposed metric, fluorine densification energy (FDE), which quantifies interaction strength in fluorine domains and correlates with C–F bond count. Lower FDE reduces N_2 -anion dissociation energy while increasing free volume, thereby enhancing solubility. Medium-to-long fluorinated alkyl chains within a polar environment form distinct domains, further emphasizing FDE's role in improving N_2 solubility.[84]

These findings provide a valuable basis for designing ILs tailored for efficient N_2 capture and conversion. In the context of this review, the cited work highlights the critical interconnection between understanding the nonstructural organization of ILs, elucidating molecular interactions at the atomic level, and applying this fundamental knowledge to develop fit-for-purpose solvents.

Ionic liquids and the 21st-century chemistry

One of the major concerns in modern chemistry and chemical engineering is the urgent need to rethink chemical processes to ensure a more sustainable and responsible use of natural resources. A formal acknowledgment of this necessity can be found in Principle No. 7 of the Green Chemistry Decalogue,[85–87] which advocates for the use of renewable feedstocks. This principle is particularly impactful in organic and polymer chemistry, where fossil-based carbon sources remain the primary raw materials.

A virtually limitless reservoir of renewable chemical feedstocks for a redesigned, sustainable chemistry is represented by lignocellulosic waste – such as sugarcane bagasse, wheat straw, rice straw, corn husks, and stover – which is produced in vast quantities each year but is only partially utilized for value-added products, aside from biofuel production.[88] Using cellulose, for instance, as a carbon source in chemical processes instead of petroleum derivatives could contribute to carbon-neutral chemistry, given that CO_2 is reabsorbed during the natural regeneration of cellulose. However, despite its potential, this shift is hampered by cellulose's intrinsic recalcitrance to dissolution and chemical transformation, necessitating a multi-step approach to effectively process biomass-derived materials. This chemical stability arises from the complex three-dimensional architecture of lignocellulosic materials, where cellulose, hemicellulose, and lignin form microfibrillar units that provide both chemical and mechanical robustness.[89] A key step in utilizing cellulose as a chemical precursor involves its degradation into furan derivatives (Fig. 18),[90] with particular attention given to 2-hydroxymethylfurfural (HMF). HMF has recently been described as a "sleeping giant"[91] due to its transformative potential in the shift toward non-petroleum-based chemistry – one of the most promising scenarios for 21st-century chemical innovation.[92]

The first challenge in cellulose processing is its solubilization, which traditionally relies on derivatizing agents – such as NaOH and CS_2 in the "Viscose" process, which produces cellulose xanthogenates – or non-derivatizing solvents, like N-methylmorpholine-N-oxide in the "Lyocell" process.[93] While extensively studied,[93,94] these methods often suffer from high environmental impact and/or excessive energy consumption, making the search for more sustainable alternatives imperative. A major breakthrough came in 2002, when a selected set of imidazolium-based ionic liquids (ILs) was proposed as efficient, non-derivatizing solvents for cellulose.[95] This discovery marked the beginning of a strong connection between ILs and biomass valorization, paving the way for more efficient utilization of natural waste. Systematic tests on alkylimidazolium ILs with varying alkyl chain lengths and counterions, ranging from highly hydrogen-bond-accepting chloride to large,

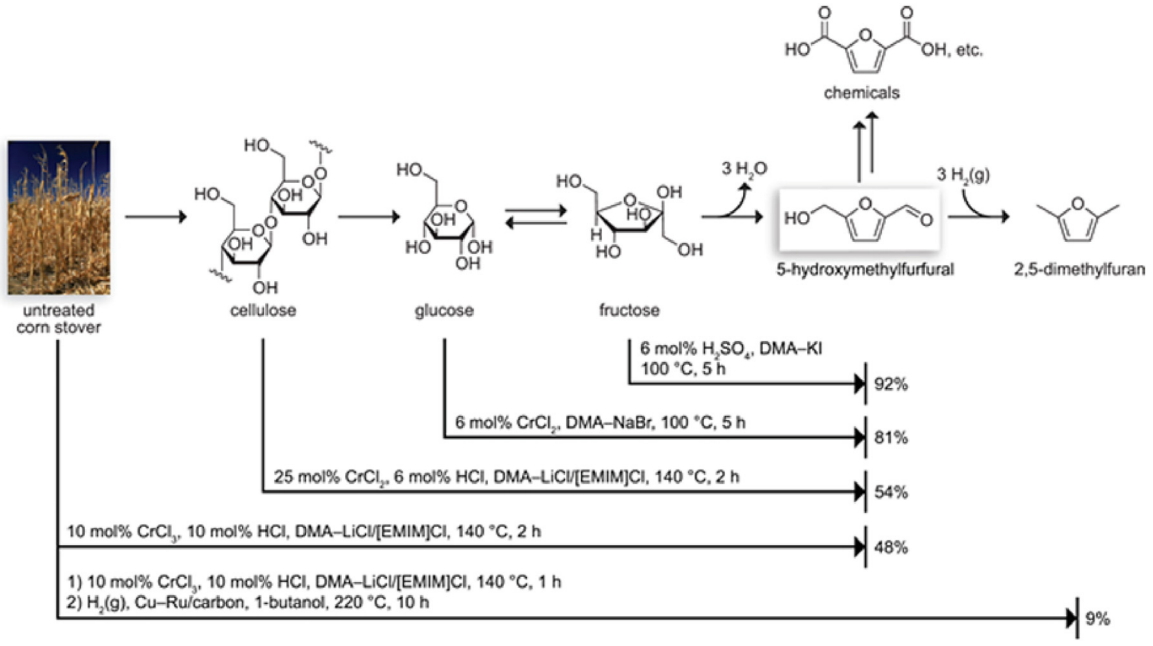

Fig. 18: Strategies for the conversion of ligno-cellulosic biomass into furane derivatives. Reprinted from ref. 90 with permission and under the terms of the Creative Commons Attribution (CC BY).

non-coordinating anions such as PF_6^-, BF_4^-, Br^-, and SCN^-, were proposed. Results revealed that chloride-based ILs with medium alkyl chain lengths – specifically [Bmim][Cl] – exhibited the highest cellulose solubility, especially when combined with microwave heating. This approach enabled the preparation of solutions containing up to 10 wt% cellulose (viscous liquid phase) and even 25 wt% cellulose (semi-solid, nematic phase).

The underlying mechanism behind this remarkable solubility was attributed to chloride anions disrupting the extensive network of hydrogen bonds that hold cellulose chains together in a compact, fibrillar structure. A conceptual sketch of this process is shown in Fig. 19. By breaking these intermolecular hydrogen bonds, the chloride ions enable individual polysaccharide chains to interact with the solvent, effectively dissolving the cellulose.[96] This solvation mechanism was elegantly confirmed through multinuclear NMR relaxation studies.[97] The approach involved monitoring the dynamic behavior of pure ILs and IL-cellulose solutions using ^{13}C and ^{35}Cl NMR relaxation times (T_1 and T_2). Since ^{13}C data reflect the dynamics of the imidazolium cation, while ^{35}Cl NMR selectively probes the chloride environment, this method provided key insights into solvent-solute interactions. As shown in Fig. 20 (top panel), the ^{13}C relaxation data indicate a transition in cation mobility from slow tumbling (T < 70 °C, spin-diffusion regime) to fast tumbling (T > 70 °C, extreme narrowing limit), as evidenced by the minimum of the T_2 curve. Meanwhile, the ^{35}Cl relaxation times decrease with temperature due to viscosity

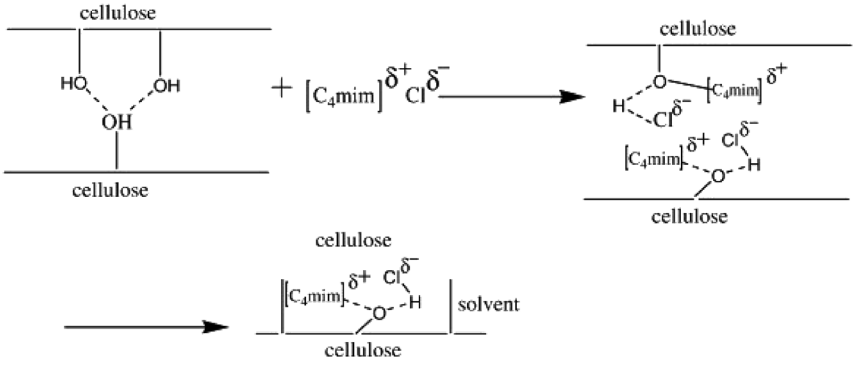

Fig. 19: Scheme of the competitive hydrogen bond action of chloride ions on the intermolecular, interchains hydrogen bonds of cellulose causing the disruption of the supramolecular organization of the cellulose strands. Reprinted with permission from ref. 96. Copyright © 2008 Elsevier B.V.

changes and ion pair formation. The central panel highlights the contrasting responses of the cation (left) and anion (right) to increasing cellobiose concentration – a disaccharide chosen as a simple model for cellulose solutes. While ^{13}C relaxation times remain largely unaffected, the ^{35}Cl data exhibit a pronounced concentration dependence, providing clear evidence of strong chloride-solute interactions.

Further confirmation comes from the bottom panel of Fig. 20, which highlights the sensitivity of the ^{35}Cl NMR linewidth profile to solvation shell symmetry, a direct consequence of the quadrupolar nature of ^{35}Cl relaxation. The spectral bands shown in Fig. 20 (bottom) exhibit significant broadening with increasing solute concentration when the solute acts as a hydrogen bond donor toward chloride. In contrast, when using peracetylated glucose – incapable of donating hydrogen bonds – the spectral lines remain sharp. These findings reinforce the pivotal role of chloride anions in cellulose dissolution, further supporting the potential of ILs as effective solvents for biomass-derived materials.[97,98] From a methodological perspective, the cellulose–alkylimidazolium chloride

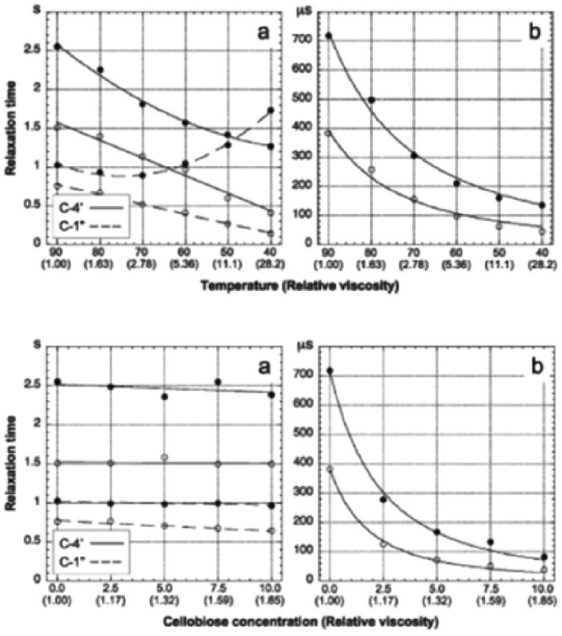

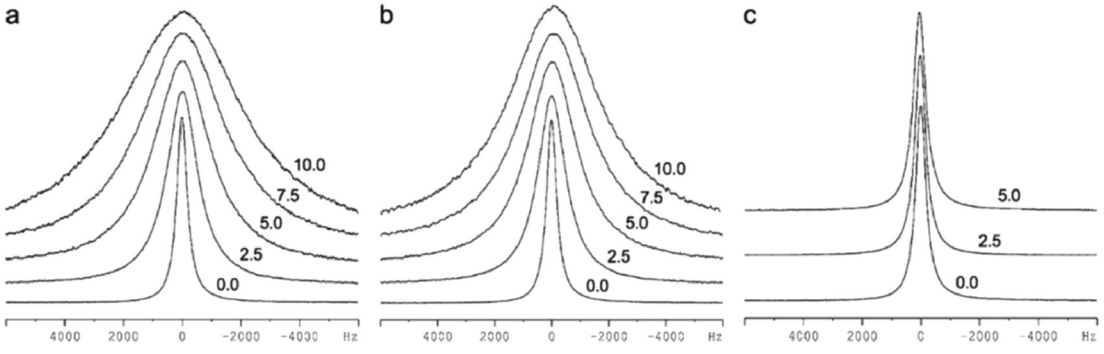

Fig. 20: Top left: ^{13}C NMR T_1 (•) and T_2 (○) relaxation times as a function of T (°C) for the N-methyl groups (C4′, full line) and methyl groups at the end of the butyl chain (C1″, dashed line) of [Bmim][Cl]. Top right: ^{35}Cl NMR T_1 (•) and T_2 (○) relaxation times for chloride ions as a function of T (K) of [Bmim][Cl]. Middle: Same as above at constant T = 90 °C as a function of cellobiose concentration mimiking the presence of cellulose (in brakets the corresponding viscosity). Bottom: Lineshape of ^{35}Cl NMR signal of chloride ions at 90 °C with increasing concentration of cellobiose (left panel), glucose (middle panel), and glucose pentaacetate (right panel) in [C_4mim]Cl. Reprinted with permission from ref. 97. Copyright © 2006 Royal Society of Chemistry.

system serves as a paradigmatic example of the unique capability of NMR spectroscopy to selectively monitor individual components within IL-based systems by appropriately tuning the observation channel (see also the previous section on NOE).

The anion's function as a hydrogen bond acceptor was thus identified as the key structural feature enabling cellulose dissolution. This insight laid the foundation for the true "rational design" of ILs – a concept frequently emphasized in the introductory sections of research articles on ILs (see Introduction). To further validate this model, Xu et al.[99] conducted a systematic study of anion basicity, providing valuable insights for the scientific community. They were the first to report Kamlet-Taft (K-T) β values for a broad set of imidazolium-based ILs, establishing a clear relationship between anion structure and its H-bond acceptor capability, as quantified by β values. Notably, they proposed a simple spectroscopic criterion to assess how efficiently the anion acts as hydrogen bond acceptor, leveraging the well-known sensitivity of the C(2)–H ^{1}H NMR chemical shift in imidazolium cations to the presence of a hydrogen bond acceptor.[100] Their study revealed a compelling linear correlation between cellulose solubility data and K-T β values, offering a practical criterion for selecting suitable ILs for cellulose dissolution. A graphical summary of this method is presented in Fig. 21.

Building upon this rational design approach, the same authors explored an additional strategy by leveraging the ability of Li^+ ions to bind to Lewis base sites, such as the hydroxyl functional groups of cellulose.[99] This interaction further weakens the intermolecular hydrogen bonds that maintain cellulose's compact structure,

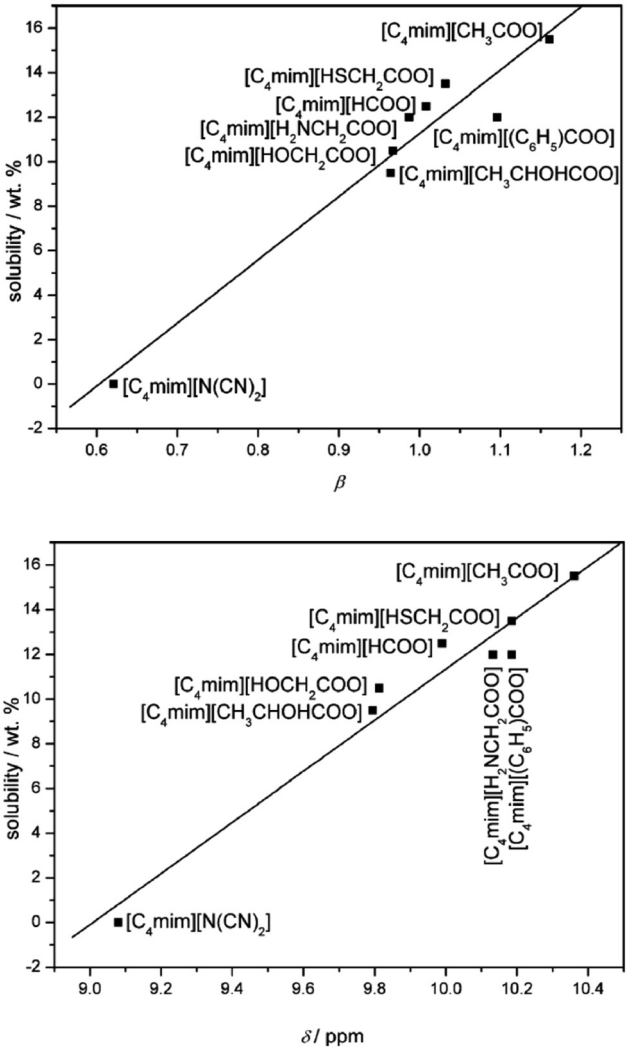

Fig. 21: Top: Correlation plot for cellulose solubility in imidazolium-based ILs and their Kamlet-Taft basicity parameter β. Bottom: Correlation between cellulose solubility imidazolium-based ILs and their ^{1}H NMR chemical shift at C(2)–H. Reprinted with permission from ref. 99. Copyright © 2010 Royal Society of Chemistry.

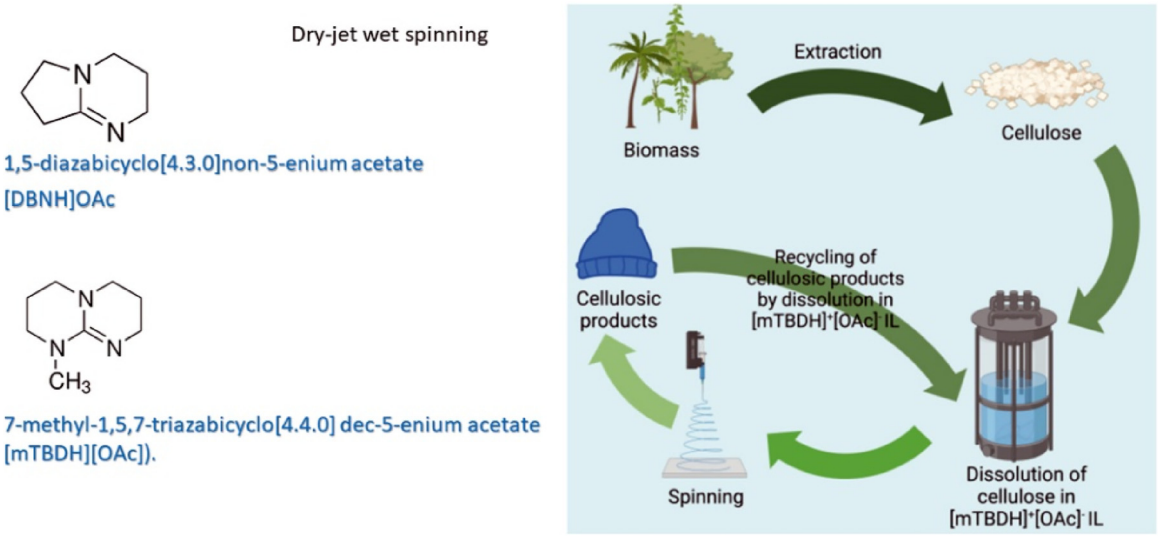

Fig. 22: Left: superbases used by the authors of refs. 102, 103 to generate ILs for cellulose fibers recycling. Right: scheme of the circular economy loop after solvent recovery. Adapted with permission from ref. 103. Copyright © 2020 American Chemical Society.

thereby enhancing its solubility. Ultimately, the combination of a basic anion – such as acetate – with the addition of Li salts creates optimal conditions for cellulose dissolution, with the added benefit that the IL can be easily recovered without decomposition after precipitation in water, used here as an antisolvent.

Now, the final piece of the puzzle comes into play: IL recyclability, a crucial factor for the sustainable application of ILs.[101] A compelling case study is provided by Sixta's research group, which investigated a recycling process for waste cotton fibers. In 2016, they successfully demonstrated a two-step process for producing man-made cellulosic fibers (MMCFs) using a Lyocell-type dry-jet wet spinning method. This approach started with a solution of post-consumer cotton fibers dissolved in a non-imidazolium-based IL.[102] The IL chosen for producing spinnable (dope) solutions was 1,5-diazabicyclo[4.3.0]non-5-enium acetate ([DBNH][OAc]), whose chemical structure is illustrated in Fig. 22. While the regenerated fibers displayed superior textile strength compared to both natural fibers and other MMCFs obtained via Lyocell-type processes, a critical limitation emerged: [DBNH][OAc] was not recyclable. After a single dissolution cycle, the IL completely lost its ability to dissolve cellulose pulp, rendering it unsuitable for reuse. To address this issue, in 2022, the researchers replaced [DBNH][OAc] with 7-methyl-1,5,7-triazabicyclo[4.4.0]dec-5-enium acetate ([mTBDH][OAc], see Fig. 22). This modification allowed quantitative solvent recovery from the coagulation bath across five consecutive cycles, without any loss of performance.[103] The optimization of solvent recycling enabled the full integration of IL technology into a circular economy framework, as depicted in Fig. 22. This study serves as a paradigmatic example of how ILs can be effectively utilized in sustainable industrial production.

Conclusions and outlook

In recent years, ionic liquids (ILs) have transitioned from academic curiosities to viable industrial tools. A comprehensive 2020 review of patents and applications emphasizes that while only a few full-scale IL-based processes have been commercialized, a substantial number are in pilot or demonstration stages – totaling over 60 patents and nearly 300 scientific reports covering chemical synthesis, gas storage, environmental remediation, and more.[104] The study highlights that economies of scale and improved production methods – such as continuous-flow synthesis and halide-free routes – are reducing costs and making ILs increasingly competitive with conventional solvents, especially when improvements in recyclability, selectivity, and safety are taken into account.[105]

What challenges lie ahead for ionic liquids in the near future? Among the many possible answers, I will focus on one that is particularly relevant today: sustainability. The early months of 2025 have seen an unpredictable yet remarkable trend in the Western world – a move to scale back the so-called Green Deal. This shift raises critical questions about the feasibility of reconciling environmental goals with labor and market dynamics (for instance, the ongoing controversy surrounding the transition from combustion engines to electric vehicles). In the context of this article, and in my personal and admittedly subjective view, the most significant challenge for ILs lies in the sustainability of the processes in which they are used.

One important example of this recent shift is the simplification package introduced by the European Commission in February 2025. This initiative postponed or reduced the scope of several sustainability-related regulations, including reporting obligations under the Corporate Sustainability Reporting Directive (CSRD), and narrowed the number of companies required to comply.[106] These changes were presented as necessary to reduce the administrative burden on businesses, but they also reflect increasing tension between environmental objectives and economic priorities. As reported by the Financial Times, this political retreat – driven in part by pressure from certain EU member states – may slow down the adoption of green technologies and weaken long-term investment signals.[107] For researchers working with ionic liquids, these developments suggest that regulatory support for sustainability can no longer be taken for granted and must be continuously reinforced by demonstrating robust, quantifiable environmental performance.

The modern vision of sustainability places two fundamental demands on the chemical community, whether focused on fundamental research or on more applied and engineering-oriented work. The first is the recognition that sustainability arises from the intersection of environmental, techno-economic, and social dimensions,[108] as illustrated in Fig. 23. The second is that sustainability must be supported by quantitative descriptors, which compels all those working with ILs – whether in the lab or in industrial development – to engage with tools such as life cycle assessment and green metrics.[109]

This Copernican revolution requires a strongly multidisciplinary approach, both from individual researchers and from research teams. A paradigmatic example helps illustrate this point: when evaluating the greenness of a process based on ILs, data on toxicity and biodegradability alone are no longer sufficient to certify it as sustainable. The accidental release of ILs into the environment can disrupt ecosystems, leading to consequences that are not only economic but also social – reaffirming the threefold nature of sustainability described above. Therefore, the design of an IL-based process must incorporate eco-toxicological tests and models,[110] which have

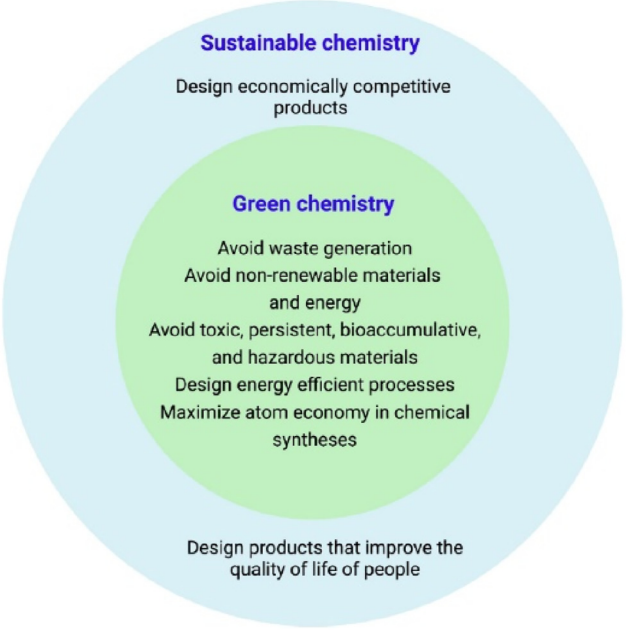

Fig. 23: The boundaries of sustainable chemistry: techno-economic, environmental and social sustainability. Reprinted with permission from ref. 104. Copyright © 2022 John Wiley and Sons.

traditionally been distant from core chemical research, in order to assess not only the effects on individual organisms but also the broader consequences for entire ecosystems.

Acknowledgments: This review originate from a plenary lecture at the The 21st IUPAC International Symposium on Solubility Phenomena and Related Equilibrium Processes (ISSP21) held at the University of Novi Sad, Serbia, in September 9-13, 2024 chaired by Prof. Slobodan Gadžurić. The author wishes to express deep gratitude to the many colleagues with whom he had the pleasure to collaborate. He is especially indebted to the numerous students, PhD candidates, and postdoctoral researchers whose immense experimental work contributed to the some of the advancements described in this review. Special thanks go to Giovanni Fronza, a mentor and source of inspiration, as well as to Franca Castiglione and Maria Enrica Di Pietro, invaluable collaborators. The author also extends his appreciation to Stefano Passerini and Giovanni Battista Appetecchi for introducing him to the applications of ILs in electrochemistry. This article is dedicated to the memory of Cinzia Chiappe, an outstanding expert in ILs, who sadly passed away in 2018.
Research ethics: Not applicable.
Informed consent: Not applicable.
Author contributions: The author has accepted responsibility for the entire content of this manuscript and approved its submission.
Use of Large Language Models, AI and Machine Learning Tools: Spelling, grammar, and style revision.
Conflict of interest: The author states no conflict of interest.
Research funding: This work was funded by the Ministero dell'Istruzione, dell'Università e della Ricerca in the framework of the PRIN2022 SEED4GREEN – Code 20223W4RT9.
Data availability: Not applicable.

References

1. Wilkes, J. S. *Green Chem.* **2002**, *4*, 73. https://doi.org/10.1039/b110838g.
2. Angell, C. A.; Ansari, Y.; Zhao, Z. *Faraday Discuss.* **2012**, *154*, 27. https://doi.org/10.1039/c1fd00112d.
3. Greaves, T. L.; Drummond, C. J. *Chem. Rev.* **2008**, *108*, 206. https://doi.org/10.1021/cr068040u.
4. Wasserscheid, P.; Keim, W. *Angew. Chem. – Intern. Ed.* **2000**, *39*, 3772. https://doi.org/10.1002/1521-3773(20001103)39:21<3772::aid-anie3772>3.0.co;2-5.
5. Armand, M.; Endres, F.; MacFarlane, D. R.; Ohno, H.; Scrosati, B. *Nat. Mater.* **2009**, *8*, 621. https://doi.org/10.1038/nmat2448.
6. Hallett, J. P.; Welton, T. *Chem. Rev.* **2011**, *111*, 3508. https://doi.org/10.1021/cr1003248.
7. Welton, T. *Chem. Rev.* **1999**, *99*, 2071. https://doi.org/10.1021/cr980032t.
8. Weingärtner, H. *Angew. Chem. – Intern. Ed.* **2008**, *47*, 654. https://doi.org/10.1002/anie.200604951.
9. Hayes, R.; Warr, G. G.; Atkin, R. *Chem. Rev.* **2015**, *115*, 6357. https://doi.org/10.1021/cr500411q.
10. Wang, Y.-L.; Li, B.; Sarman, S.; Mocci, F.; Lu, Z.-Y.; Yuan, J.; Laaksonen, A.; Fayer, M. D. *Chem. Rev.* **2015**, *120*, 5798. https://doi.org/10.1021/acs.chemrev.9b00693.
11. Pereira, J.; Souza, R.; Moreira, A.; Moita, A. *Ionics* **2024**, *30*, 4343. https://doi.org/10.1007/s11581-024-05626-x.
12. Plechkova, N. V.; Seddon, K. R. *Chem. Soc. Rev.* **2008**, *37*, 123. https://doi.org/10.1039/b006677j.
13. An excellent historical introduction to ILs can be found in: A. Mariani. *Study on Multicomponent Mixtures of Ionic Liquids and Molecular Compounds*. PhD Thesis, Sapienza Università di Roma, 2016. downloadable free of charge from https://iris.uniroma1.it/handle/11573/927689underthetermsoftheCreativeCommonsAttribution (CC BY).
14. Gabriel, S.; Weiner, J. *Ber* **1888**, *21*, 2669; https://doi.org/10.1002/cber.18880210288.
15. Walden, P. *Bull. Acad. Sci. St. Petersburg* **1914**, *405*.
16. Atkin, R.; Warr, G. G. *J. Phys. Chem. B* **2008**, *112*, 4164. https://doi.org/10.1021/jp801190u.
17. Gale, R. J.; Gilbert, B.; Osteryoung, R. A. *Inorg. Chem.* **1978**, *17*, 2728; https://doi.org/10.1021/ic50188a008.
18. Crabtree, R. H.; Hlatky, G.; Wilson, R. A.; Hu, C. L. *Inorg. Chem.* **1982**, *21*, 1273; https://doi.org/10.1021/ic00133a083.
19. Wilkes, J. S.; Zaworotko, M. J. *J. Chem. Soc. Chem. Commun.* **1992**, *965*; https://doi.org/10.1039/c39920000965.
20. Krossing, I.; Slattery, J. M.; Daguenet, C.; Dyson, P. J.; Oleinikova, A.; Weingärtner, H. *J. Am. Chem. Soc.* **2006**, *128*, 13427. https://doi.org/10.1021/ja0619612, Addition/correction https://doi.org/10.1021/ja073579a.
21. López-Martin, I.; Burello, E.; Davey, P. N.; Seddon, K. R.; Rothenberg, G. *ChemPhysChem* **2007**, *8*, 690. https://doi.org/10.1002/cphc.200600637.

22. Hardacre, C.; Holbrey, J. D.; Nieuwenhuyzen, M.; Youngs, T. G. A. *Acc. Chem. Res.* **2007**, *40*, 1146. https://doi.org/10.1021/ar700068x.
23. Canongia Lopes, J. N. A.; Pádua, A. A. H. *J. Phys. Chem. B* **2006**, *110*, 3330. https://doi.org/10.1021/jp056006y.
24. Triolo, A.; Russina, O.; Bleif, H.-J.; Di Cola, E. *J. Phys. Chem. B* **2007**, *111*, 4641. https://doi.org/10.1021/jp067705t.
25. Kashyap, H. K.; Hettige, J. J.; Annapureddy, H. V. R.; Margulis, C. J. *Chem. Commun.* **2012**, *48*, 5103. https://doi.org/10.1039/C2CC30609C.
26. Araque, J. C.; Hettige, J. J.; Margulis, C. J. *J. Phys. Chem. B* **2015**, *119*, 12727. https://doi.org/10.1021/acs.jpcb.5b05506.
27. Russina, O.; Lo Celso, F.; Di Michiel, M.; Passerini, S.; Appetecchi, G. B.; Castiglione, F.; Mele, A.; Caminiti, R.; Triolo, A. *Faraday Discuss*. **2013**, *167*, 499. https://doi.org/10.1039/c3fd00056g.
28. Overhauser, A. W. *Phys. Rev.* **1953**, *92*, 411; https://doi.org/10.1103/physrev.92.411.
29. Some Fascinating Notes on the Biography of Albert Overhauser Can Be Found at This Page of Perdue University, https://www.physics.purdue.edu/about/history/albert_w_overhauser.html.
30. Neuhaus, D.; Williamson, M. P. *The Nuclear Overhauser Effect in Structural and Conformational Analysis*; V.C.H. Publishers: New York, 1989.
31. Noggle, J. H.; Schirmer, R. E. *The Nuclear Overhauser Effect. Chemical Applications*; Academic Press: New York, 1971.
32. Wüthrich, K. *NMR of Proteins and Nucleic Acids*; John Wiley & Sons: New York, 1986.
33. Mantz, R. A.; Trulove, P. C.; Carlin, R. T.; Osteryoung, R. A. *Inorg. Chem.* **1995**, *34*, 3846. https://doi.org/10.1021/ic00118a042.
34. Mele, A.; Tran, C. D.; De Paoli Lacerda, S. H. *Angew. Chem. – Intern. Ed.* **2003**, *42*, 4364. https://doi.org/10.1002/anie.200351783.
35. Mele, A. In *Ionic Liquids IIIA: Fundamentals, Progress, Challenges, and Opportunities*; Rogers, R. D.; Seddon, K. R., Eds., cp.1, ACS Symposium Series 901: Washington DC, 2005.
36. Mele, A.; Romanò, G.; Giannone, M.; Ragg, E.; Fronza, G.; Raos, G.; Marcon, V. *Angew. Chem. – Intern. Ed.* **2006**, *45*, 1123. https://doi.org/10.1002/anie.200503745.
37. Lingscheid, Y.; Arenz, S.; Giernoth, R. *ChemPhysChem* **2012**, *13*, 261. https://doi.org/10.1002/cphc.201100622.
38. Weingärtner, H. *Personal Communication at COIL-5*: Portugal, 2013.
39. Ayant, Y.; Belorizky, E.; Fries, P.; Rosset, J. *J. Phys. Fr.* **1977**, *38*, 325. https://doi.org/10.1051/jphys:01977003803032500.
40. Nordstierna, L.; Yushmanov, P. V.; Furo, I. *J. Chem. Phys.* **2006**, *125*, 074704. https://doi.org/10.1063/1.2336199.
41. Nordstierna, L.; Yushmanov, P. V.; Furo, I. *J. Phys. Chem. B* **2006**, *110*, 25775. https://doi.org/10.1021/jp0647885.
42. Gerig, J. T. *J. Org. Chem.* **2003**, *68*, 5244. https://doi.org/10.1021/jo026599y.
43. Gerig, J. T. *J. Am. Chem. Soc.* **2005**, *127*, 9277. https://doi.org/10.1021/ja042314i.
44. Halle, B. *J. Chem. Phys.* **2003**, *119*, 12372. https://doi.org/10.1063/1.1625632.
45. Frezzato, D.; Rastrelli, F.; Bagno, A. *J. Phys. Chem. B* **2006**, *110*, 5676. https://doi.org/10.1021/jp0560157.
46. Bagno, A.; Rastrelli, F.; Saielli, G. *Prog. Nucl. Magn. Reson. Spectrosc.* **2005**, *47*, 41. https://doi.org/10.1016/j.pnmrs.2005.08.001.
47. Gabl, S.; Steinhauser, O.; Weingärtner, H. *Angew. Chem. – Intern. Ed.* **2013**, *52*, 9242. https://doi.org/10.1002/anie.201302712.
48. Martin, P.-A.; Salager, E.; Forsyth, M.; O'Dell, L. A.; Deschamps, M. *M. Phys. Chem. Chem. Phys.* **2018**, *20*, 13357. https://doi.org/10.1039/c8cp00911b.
49. Gyabeng, D.; Martin, P.-A.; Pal, U.; Deschamps, M.; Forsyth, M.; O'Dell, L. A. *Front. Chem.* **2019**, *7*, 4. https://doi.org/10.3389/fchem.2019.00004.
50. Gyabeng, D.; Qiao, L.; Zhang, H.; Oteo, U.; Armand, M.; Forsyth, M.; Chen, F.; O'Dell, L. A. *J. Mol. Liq.* **2021**, *327*, 114879. https://doi.org/10.1016/j.molliq.2020.114879.
51. Castiglione, F.; Appetecchi, G. B.; Passerini, S.; Panzeri, W.; Indelicato, S.; Mele, A. *J. Mol. Liq.* **2015**, *210*, 215. https://doi.org/10.1016/j.molliq.2015.05.036.
52. Martin, P.-A.; Chen, F.; Forsyth, M.; Deschamps, M.; O'Dell, L. A. *J. Phys. Chem. Lett.* **2018**, *9*, 7072. https://doi.org/10.1021/acs.jpclett.8b03021.
53. Honegger, P.; Di Pietro, M. E.; Castiglione, F.; Vaccarini, C.; Quant, A.; Steinhauser, O.; Schröder, C.; Mele, A. *J. Phys. Chem. Lett.* **2021**, *12*, 8658. https://doi.org/10.1021/acs.jpclett.1c02253.
54. Lo Celso, F.; Yoshida, Y.; Castiglione, F.; Ferro, M.; Mele, A.; Jafta, C.; Triolo, A.; Russina, O. *Phys. Chem. Chem. Phys.* **2017**, *19*, 13101. https://doi.org/10.1039/c7cp01971h.
55. Di Pietro, M. E.; Goloviznina, K.; van den Bruinhorst, A.; de Araujo Lima e Souza, G.; Costa Gomes, M.; Padua, A. A. H.; Mele, A. *ACS Sustainable Chem. Eng.* **2022**, *10*, 11835. https://doi.org/10.1021/acssuschemeng.2c02460.
56. Lingscheid, Y.; Paul, M.; Bröhl, A.; Neudörfl, J. M.; Giernoth, R. *Magn. Reson. Chem.* **2018**, *56*, 80. https://doi.org/10.1002/mrc.4608.
57. Zanatta, M.; Dupont, J.; Wentz, G. N.; dos Santos, F. P. *Phys. Chem. Chem. Phys.* **2018**, *20*, 11608. https://doi.org/10.1039/c8cp00066b.
58. Romeo, L. M.; Bolea, I.; Escosa, J. M. *Appl. Therm. Eng.* **2008**, *28*, 1039. https://doi.org/10.1016/j.applthermaleng.2007.06.036.
59. Karadas, F.; Atilhan, M.; Aparicio, S. *Energy Fuels* **2010**, *24*, 5817. https://doi.org/10.1016/10.1021/ef1011337.
60. Blanchard, L. A.; Hancu, D.; Beckman, E. J.; Brennecke, J. F. *Nature* **1999**, *399*, 29. https://doi.org/10.1038/19887.
61. Hasib-ur-Rahman, M.; Siaj, M.; Larachi, F. *Chem. Eng. Proc.* **2010**, *49*, 313; https://doi.org/10.1016/j.cep.2010.03.008.
62. Bara, J. E.; Carlisle, T. K.; Gabriel, C. J.; Camper, D.; Finotello, A.; Gin, D. L.; Noble, R. D. *Ind. Eng. Chem. Res.* **2009**, *48*, 2739. https://doi.org/10.1021/ie8016237.
63. Hu, Y.-F.; LiuXuZhang, Z. C. C. M. X. M.; Xu, C.-M.; Zhang, X.-M. *Chem. Soc. Rev.* **2011**, *40*, 3802. https://doi.org/10.1039/C0CS00006J.
64. Bara, J. E.; Camper, D.; Gin, D. L.; Noble, R. D. *Acc. Chem. Res.* **2010**, *43*, 152. https://doi.org/10.1021/ar9001747.
65. Jessop, P. G.; Heldebrant, D. J.; Li, X.; Eckert, C. A.; Liotta, C. L. *Nature* **2005**, *436*, 1102. https://doi.org/10.1038/4361102a.
66. Wang, C.; Mahurin, S. M.; Luo, H.; Baker, G. A.; Li, H.; Dai, S. *Green Chem.* **2010**, *12*, 870. https://doi.org/10.1039/b927514b.
67. Wang, C.; Luo, H.; Luo, X.; Li, H.; Dai, S. *Green Chem.* **2010**, *12*, 2019. https://doi.org/10.1039/c0gc00070a.

68. Cadena, C.; Anthony, J. L.; Shah, J. K.; Morrow, T. I.; Brennecke, J. F.; Maginn, E. J. *J. Am. Chem. Soc.* **2004**, *126*, 5300. https://doi.org/10.1021/ja039615x.
69. Huang, X.; Margulis, C. J.; Li, Y.; Berne, B. J. *J. Am. Chem. Soc.* **2005**, *127*, 17842. https://doi.org/10.1021/ja055315z.
70. See, as an example. Ruocco, G.; Sampoli, M.; VallauriVallauri, R. *J. Chem. Phys.* **1992**, *96*, 6167. and references therein https://doi.org/10.1063/1.462889.
71. Shelepova, E. A.; Medvedev, N. N. *J. Mol. Liq.* **2022**, *349*, 118127. https://doi.org/10.1016/j.molliq.2021.118127.
72. Yampolskii, Y. P. *Russ. Chem. Rev.* **2007**, *76*, 59. https://doi.org/10.1070/RC2007v076n01ABEH003629.
73. Dlubek, G.; Yang, Yu; Krause-Rehberg, R.; Beichel, W.; Bulut, S.; Pogodina, N.; Krossing, I.; Friedrich, Ch. *J. Chem. Phys.* **2010**, *113*, 124502. https://doi.org/10.1063/1.3487522.
74. Yu, Y.; Beichel, W.; Dlubek, G.; Krause-Rehberg, R.; Paluch, M.; Pionteck, J.; Pfefferkorn, D.; Bulut, S.; Friedrich, C.; Pogodina, N.; Krossing, I. *Phys. Chem. Chem. Phys.* **2012**, *14*, 6856. https://doi.org/10.1039/c2cp40486a.
75. Beichel, W.; Yu, Y.; Dlubek, G.; Krause-Rehberg, R.; Pionteck, J.; Pfefferkorn, D.; Bulut, S.; Bejan, D.; Friedrich, C.; Krossing, I. *Phys. Chem. Chem. Phys.* **2013**, *15*, 8821. https://doi.org/10.1039/c3cp43306d.
76. Morgado, P.; Shimizu, K.; Esperança, J. M. S. S.; Reis, P. M.; Rebelo, L. P. N.; Canongia Lopes, J. N.; Filipe, E. J. M. *J. Phys. Chem. Lett.* **2013**, *4*, 2758. https://doi.org/10.1021/jz401279u.
77. Castiglione, F.; Simonutti, R.; Mauri, M.; Mele, A. *J. Phys. Chem. Lett.* **2013**, *4*, 1608. https://doi.org/10.1021/jz400617v.
78. Brooks, N. J.; Castiglione, F.; Doherty, C. M.; Dolan, A.; Hill, A. J.; Hunt, P. A.; Matthews, R. P.; Mauri, M.; Mele, A.; Simonutti, R.; Villar-Garcia, I. J.; Weber, C. C.; Welton, T. *Chem. Sci.* **2017**, *8*, 6359. https://doi.org/10.1039/c7sc01407d.
79. Chen, J. G.; Crooks, R. M.; Seefeldt, L. C.; Bren, K. L.; Bullock, R. M.; Darensbourg, M. Y.; Holland, P. L.; Hoffman, B.; Janik, M. J.; Jones, A. K.; Kanatzidis, M. G.; King, P.; Lancaster, K. M.; Lymar, S. V.; Pfromm, P.; Schneider, W. F.; Schrock, R. R. *Science* **2018**, *360*, eaar6611. https://doi.org/10.1126/science.aar6611.
80. Shen, H.; Choi, C.; Masa, J.; Li, X.; Qiu, J.; Jung, Y.; Sun, Z. *Chem.* **2021**, *7*, 1708. https://doi.org/10.1016/j.chempr.2021.01.009.
81. Almantariotis, D.; Pensado, A. S.; Gunaratne, H. Q. N.; Hardacre, C.; Pádua, A. A. H.; Coxam, J.-Y.; Costa Gomes, M. F. *J. Phys. Chem. B* **2017**, *121*, 426. https://doi.org/10.1021/jpcb6b10301.
82. Kang, C. S. M.; Zhang, X.; MacFarlane, D. R. *J. Phys. Chem. C* **2018**, *122*, 24550. https://doi.org/10.1021/jpcc8b07752.
83. Kang, C. S. M.; Zhang, X.; MacFarlane, D. R. *J. Phys. Chem. C* **2019**, *123*, 21376. https://doi.org/10.1021/jpcc9b06000.
84. Li, K.; Wang, Y.; Wang, C.; Huo, F.; Zhang, S.; He, H. *J. Am. Chem. Soc.* **2024**, *146*, 25569. https://doi.org/10.1021/jacs.4c06784.
85. Anastas, P. T.; Warner, J. C. *Green Chemistry: Theory and Practice*; Oxford University Press: Oxford, 1998.
86. Anastas, P. T.; Kirchhoff, M. M. *Acc. Chem. Res.* **2002**, *35*, 686. https://doi.org/10.1021/ar010065m.
87. A Pocket Guide is Dowloadable Here: https://www.acs.org/greenchemistry/principles/12-principles-of-green-chemistry.html.
88. Roy, S.; Chundawat, S. P. S. *BioEnergy Res.* **2023**, *16*, 263. https://doi.org/10.1007/s12155-022-10425-1.
89. Sorek, N.; Yeats, T. H.; Szemenyei, H.; Youngs, H.; Somerville, C. R. *BioScience* **2014**, *64*, 192. https://doi.org/10.1093/biosci/bit037.
90. Binder, J. B.; Raines, R. T. *J. Am. Chem. Soc.* **2009**, *131*, 1979. https://doi.org/10.1021/ja808537j.
91. Galkin, K. I.; Ananikov, V. P. *ChemSusChem* **2019**, *12*, 2976. https://doi.org/10.1002/cssc.201900592.
92. Mori, R. *RSC Sustainability* **2023**, *1*, 179. https://doi.org/10.1039/d2su00014h.
93. Clough, M. T. *Green Chem.* **2017**, *19*, 4754. https://doi.org/10.1039/c7gc01776f.
94. Nawaz, H.; He, A.; Wu, Z.; Wang, X.; Jiang, Y.; Ullah, A.; Xu, F.; Xie, F. *Int. J. Biol. Macromol.* **2024**, *273*, 133012. https://doi.org/10.1016/j.ijbiomac.2024.133012.
95. Swatloski, R. P.; Spear, S. K.; Holbrey, J. D.; Rogers, R. D. *J. Am. Chem. Soc.* **2002**, *124*, 4974. https://doi.org/10.1021/ja025790m.
96. Feng, L.; Chen, Z. *J. Mol. Liq.* **2008**, *142*, 1. https://doi.org/10.1016/j.molliq.2008.06.007.
97. Remsing, R. C.; Swatloski, R. P.; Rogers, R. D.; Moyna, G. *Chem. Commun.* **2006**, *1271*. https://doi.org/10.1039/b600586c.
98. Wang, H.; Gurau, G.; Rogers, R. D. *Chem. Soc. Rev.* **2012**, *41*, 1519. https://doi.org/10.1039/c2cs15311d.
99. Xu, A.; Wang, J.; Wang, H. *Green Chem.* **2010**, *12*, 268. https://doi.org/10.1039/b916882f.
100. Lungwitz, R.; Spange, S. *New J. Chem.* **2008**, *32*, 392. https://doi.org/10.1039/b714629a.
101. Khoo, Y. S.; Tjong, T. C.; Chew, J. W.; Hu, X. *Sci. Total Environ.* **2024**, *922*, 171238. https://doi.org/10.1016/j.scitotenv.2024.171238.
102. Asaadi, S.; Hummel, M.; Hellsten, S.; Härkäsalmi, T.; Ma, Y.; Michud, A.; Sixta, H. *ChemSusChem* **2016**, *9*, 3250. https://doi.org/10.1002/cssc.201600680.
103. Elsayed, S.; Hellsten, S.; Guizani, C.; Witos, J.; Rissanen, M.; Rantamäki, A. H.; Varis, P.; Wiedmer, S. K.; Sixta, H. *ACS Sustainable Chem. Eng.* **2020**, *8*, 14217. https://doi.org/10.1021/acssuschemeng.0c05330.
104. Pešić, J.; Watson, M.; Papović, S.; Vraneš, M. *Recent Pat. Nanotechnol.* **2021**, *15*, 225. https://doi.org/10.2174/1872210513999190923121448.
105. Greer, A. J.; Jacquemin, J.; Hardacre, C. *Molecules* **2020**, *25*, 5207. https://doi.org/10.3390/molecules25215207.
106. https://ec.europa.eu/commission/presscorner/detail/en/ip_25_614.
107. https://www.ft.com/content/36c48615-3fa8-4e28-8729-682f6f3fbe55.
108. Quintana, A. A.; Sztapka, A. M.; Santos Ebinuma, V. d. C.; Agatemor, C. *Angew. Chem. – Intern. Ed.* **2022**, *61*, e202205609. https://doi.org/10.1002/anie.202205609.
109. Baaqel, H. A.; Bernardi, A.; Hallett, J. P.; Guillen-Gosalbez, G.; Chachuat, B. *ACS Sustainable Chem. Eng.* **2023**, *11*, 7157. https://doi.org/10.1021/acssuschemeng.3c00547.
110. Kaur, N.; Mithu, V. S.; Kumar, S. *J. Mol. Liq.* **2024**, *397*, 124095. https://doi.org/10.1016/j.molliq.2024.124095.